Acta Geotechnica (2023) 18:2239–2261
https://doi.org/10.1007/s11440-022-01664-9

RESEARCH PAPER

Microscale investigations of temperature-dependent microbially induced carbonate precipitation (MICP) in the temperature range 4–50 °C

Yuze Wang[1,2] · Yong Wang[2] · Kenichi Soga[3] · Jason T. DeJong[4] · Alexandre J. Kabla[5]

Received: 24 February 2022 / Accepted: 27 July 2022 / Published online: 31 October 2022

Abstract

Microbially induced carbonate precipitation (MICP) involves a series of bio-geochemical reactions whereby microbes alter the surrounding aqueous environment and induce calcium carbonate precipitation. MICP has a broad range of applications, including in situ soil stabilization. However, the reliability of this process is dependent on a number of environmental conditions. In particular, bacterial growth, urease activity and precipitation kinetics all depend on temperature. Batch test and microfluidic chip experiments were performed in this study to investigate the effects of temperature on bacterial density and activity and the MICP processes occurring at different temperatures (4–50 °C). Spatial and temporal variations in the formation and development of calcium carbonate precipitates, including their amount, type, growth rate, formation and deformation characteristics, were monitored. Results show that different types of calcium carbonate precipitates with varying sizes and quantities were produced by varying the temperature. Low temperature (4 °C) did not reduce urease activity, but limited the final amount of cementation; low temperature reduced bacterial growth and attachment ratio, as well as calcium carbonate precipitation rate. High-temperature (50 °C) conditions significantly reduced urease activity within a short period of time, while a repeated injection of bacteria before every two injections of cementation solution increased the final amount of cementation. The findings made from this paper provide insight into how MICP processes vary across a range of temperatures and could be valuable for optimizing the MICP process for different applications.

Keywords Crystal growth · Crystal dissolution · MICP · Microfluidic chip · Temperature effects

Abbreviations

MICP	Microbially induced carbonate precipitation
BS	Bacterial suspension
CS	Cementation solution
YE	Yeast extract

✉ Yuze Wang
wangyz@sustech.edu.cn

1 Shenzhen Key Laboratory of Natural Gas Hydrates, Southern University of Science and Technology, Shenzhen 518055, China

2 Department of Ocean Science and Engineering, Southern University of Science and Technology, Shenzhen 518055, China

3 Department of Civil and Environmental Engineering, University of California, Berkeley, CA 94720, USA

4 Department of Civil and Environmental Engineering, University of California, Davis, CA 95616, USA

5 Department of Engineering, University of Cambridge, Cambridge CB2 1PZ, UK

1 Introduction

Microbially induced carbonate precipitation (MICP), particularly via the urea hydrolysis pathway, has been extensively studied for its potential subsurface applications including permeability reduction of porous and fractured medium [2, 27], soil stabilization [7, 12, 29, 40] and environmental remediation [1], Jiang et al. [28]. During MICP treatment, bacteria with ureolytic activity produce a urease enzyme that catalyzes the hydrolysis of urea (Eq. 1). The addition of calcium (Ca^{2+}) to this system then induces precipitation of calcium carbonate ($CaCO_3$) as CO_3^{2-} ions react with Ca^{2+} (Eq. 2):

$$CO(NH_2)_2 + 2H_2O \xrightarrow{Urease} 2NH_4^+ + CO_3^{2-} \quad (1)$$

$$Ca^{2+} + CO_3^{2-} \rightarrow CaCO_3(s) \quad (2)$$

The precipitated calcium carbonates produced by these in situ biochemical reactions have multiple functions in porous soil media, such as reducing pore space, bonding soil particles and co-precipitating with heavy metals or radionuclides.

The reactions do not only depend on the quantity and activity of bacteria [37], and the content and concentration of cementation solution [2], [44], but also on the environmental parameters such as temperature, pH, saturation conditions and salinity [15, 17, 26, 33]. Therefore, understanding the effects of environmental factors on the biochemical reactions is needed to predict and control the formation of $CaCO_3$ crystals which affects the engineering properties of MICP-treated soils.

Temperature is one of the most important environmental factors to consider. In addition to affecting bacterial growth, death and activity which consequently influences the rate of urea hydrolysis (Eq. 1), temperature also affects the rate of precipitation (Eq. 2) and the amount and morphology of the $CaCO_3$ crystals formed. Most previous MICP studies were conducted at room temperatures (20–25 °C), whereas the temperature in the engineering field varies [6, 9, 19]. For instance, if MICP is used to mitigate sand production during methane gas extraction from hydrate-bearing soils, the operational temperature could be between 0 and 12 °C [23, 30, 32],if MICP is applied to seal the fractures of geoformation for CO_2 storage, the temperature in the deep subsurface could be higher than 31 °C [25],when MICP is used to stabilize subsurface soils in arid regions in hot summer, the soil temperature may be as high as 50 °C [18, 42].

Some of the previously published studies have examined the effect of temperature on crystals characteristics, carbonate amount and the strength improvement of MICP-treated soils. Cheng et al. [8] conducted soil column experiments and showed that compared with 25 °C, either low (4 °C) or high (50 °C) temperature results in the formation of relatively smaller calcium carbonate crystals compared to the size of crystals produced at 25 °C. The reasons for the production of smaller calcium carbonate crystals are assumed to be because of low urease activity at 4 °C, and larger numbers of crystal nucleation produced at 50 °C [8]. Sun et al. [34] suggested that, in the range of 15–30 °C, higher temperature can precipitate more calcium carbonate within 48 h, because bacterial reproduction and enzyme activity increase at higher temperatures which results in increased precipitation efficiency. By contrast, Peng et al. [31] conducted batch tests and reported that the urea hydrolysis activity of bacterial suspensions increased to a peak and then decreased over time within 400 h, and the higher the temperature, the faster the activity decreased. In addition, by conducting soil column experiments, Peng et al. [31] found that in the temperature range of 10–30 °C, higher temperatures resulted in less precipitation of $CaCO_3$.

In the light of these results, it is necessary to further investigate the effect of temperature on urease activity and the dynamics of $CaCO_3$ precipitation. Earlier studies have shown that bacterial density, which may change due to their in situ growth, detachment and death during the MICP treatment procedure [38], significantly affects crystal number and characteristics [37]. In this study, we deploy a similar approach to further examine the role of temperature. A series of batch tests were conducted to study the effects of temperature on bacterial population and activity. In addition, microfluidic chip experiments were conducted to observe the MICP processes at the pore scale at different temperatures between 4 to 50 °C. The implications of the findings in terms of resulting engineering properties and treatment protocols for subsurface applications of MICP are also discussed.

2 Materials and methods

2.1 Bacterial suspension

Sporosarcina pasteurii (DSM 33) was used in the experiments described in this study. Bacterial suspension was prepared using a freeze-dried stock, which was activated according to the supplier's guidelines (DSM). After activation, glycerol stocks of the bacteria were prepared by adding 225 µl of 80% glycerol (autoclaved) to 1 ml of overnight liquid culture in cryogenic vials, after which the liquid culture was immediately frozen at − 80 °C [36]. Once defrosted, cells from the glycerol stock were grown in ATCC 1376 NH_4-YE agar medium (20 g/L yeast extract, 10 g/L ammonium sulfate, 20 g/L agar and 0.13 M Tris base) for 48 h at 30 °C. Subsequently, several colonies on the agar plate were transferred to a NH_4-YE liquid medium containing the same components without agar and cultivated in a shaking incubator for 24 h at 30 °C and a shaking rate of 200 rpm to obtain a bacterial suspension with an optical density measured at a wavelength of 600 nm (OD_{600}) of around 3.0. The bacterial suspension with OD_{600} of 1.0 that was used in the experiments was diluted from this bacterial suspension using NH_4-YE liquid medium. Based on the results obtained by Wang et al. [37], the correlation between bacterial number per unit volume, denoted as CB, and bacterial optical density OD_{600} is:

$$C_B = \text{Bacterial density of cells(cells/ml)} = \text{OD}_{600} \times 4 \times 10^8 \quad (3)$$

2.2 Batch test and urease activity measurement

Bacteria were cultivated in NH_4-YE liquid following the same procedure described in the previous section, to OD_{600} of about 1.0. The bacterial suspension was subsequently divided equally into 12 bottles, with each of the bottle containing about 100 ml of bacterial suspension. Three bottles of bacterial suspension were incubated without shaking at a temperature of either 4, 20, 35, or 50 °C. To measure the urease activity, 2 ml of bacterial suspension were removed from each of the bottles after every 12 to 24 h to measure OD_{600}. After measuring OD_{600}, 1 ml from this 2 ml was mixed with 9 ml of 1.1 mol/L urea for 5 min to measure the conductivity change and to obtain the ureolysis rate (Whiffin 2007). In addition, as a comparison, urease activity was measured at a different temperature to quantify the effects of temperature on urease activity. In this experiment, 1 ml of bacterial suspension was mixed with 9 ml of 1.1 mol/L urea and placed at various temperatures ranging from 5 to 70 °C for 5 min to measure the conductivity. The conductivity of the mixed content was assessed using a conductivity meter (FiveGo, Mettler-Toledo, Beaumont Leys, Leicester, UK) immediately after the mixing and 5 min after mixing. The ureolysis rate was calculated using Eq. (4) [40]. Measurements were performed in triplicate for each of the different media tested, with data presented as mean ± standard error.

$$\mathrm{U(mM/h)} = \frac{\Delta\mathrm{Conductivity}(\mu S/cm)}{\Delta t(\mathrm{min})} \times (10^{-3} \times 11.11)(mM/(\mu S/cm)) \times 60(\mathrm{min}/h) \quad (4)$$

The specific urease activity of bacteria was calculated using Eq. (5)

$$U'(mM/h) = \frac{U(mM/h)}{OD_{600}}(mM/h/OD_{600}) \quad (5)$$

2.3 Cementation solution

The cementation solution for MICP treatment was created using calcium chloride ($CaCl_2$), urea ($CO(NH_2)_2$) and a nutrient broth dissolved in deionized water. The urea and calcium chloride served as important ingredients for promoting calcite precipitation, and the nutrient broth served as an energy source for urease activity. The concentrations of $CaCl_2$, urea and nutrient broth were 0.5 M, 0.75 M and 3 g/L, respectively [36].

2.4 Microfluidic chip experiments and MICP treatment

Microfluidic chip experiments were performed to observe the MICP process in a porous medium under conditions that are affected by flow rate and injection methods [38]. The microfluidic chips were designed to create a two-dimensional model of a realistic soil matrix porous structure based on a cross-sectional image of Ottawa 50–70 soil and were fabricated using standard photolithograph techniques. The details of the device and its fabrication process can be found in Wang et al. [39] and Wang et al. [38]. Because the microfluidic chip is transparent, the MICP process inside the microfluidic chip can be observed under a microscope. The schematic of the microfluidic chip experiments is shown in Fig. 1. Except during bacterial injection (Fig. 1a), cementation solution injection (Fig. 1a) and imaging (Fig. 1c), all samples were kept at the assigned temperatures (Fig. 1b).

In total 6 tests were conducted (Table 1). Tests 1–4 were conducted to compare the effects of temperature on MICP. Test 5 was conducted to be compared with Test 4 for investigating the effects of settling time and injection interval of cementation solution on MICP. Test 6 was used to compare with Test 5 for investigating the effects of injection number of bacterial suspension on MICP. In each of the test, after microfluidic chips were made and saturated with deionized water, one pore volume of bacterial suspension with an OD_{600} of 1.0 was injected into each of the microfluidic chip samples at a flow rate of 0.5 ml/h (Darcy velocity of 4.6×10^{-4} m/s) for two minutes at room temperature (20 °C). The samples were then incubated at different temperature conditions for bacterial settling (Table 1). After settling, in Tests 1–5, ten staged injections of cementation solution at a flow rate of 0.05 ml/h (Darcy velocity of 4.6×10^{-5} m/s) were conducted. The interval between injections of cementation solution for Tests 1–4 was 48 h, whereas that for Test 5 was $6 \sim 18$ h. In Test 6, bacterial injection was performed before every two injections of cementation solution and five injections were performed in total.

After the MICP treatment procedures were completed, images of samples were taken by an optical microscope (Zeiss Axio Observer Z1) to visualize the microscale MICP process (Fig. 1c). The microscope was equipped with a digital video camera (Zeiss Axio Observer Z1) connected to a computer. The bacterial cell numbers in the image of one central pore of the microfluidic chips taken after bacterial injection, after bacterial settling and after the injections of cementation solution were counted to quantify the effects of temperature on bacterial growth, attachment and detachment.

2.5 Image quantification

Two types of $CaCO_3$ crystals were mostly reported in previous studies, namely spherical and rhombohedral crystals [36, 37]. The observed $CaCO_3$ crystals that grow in

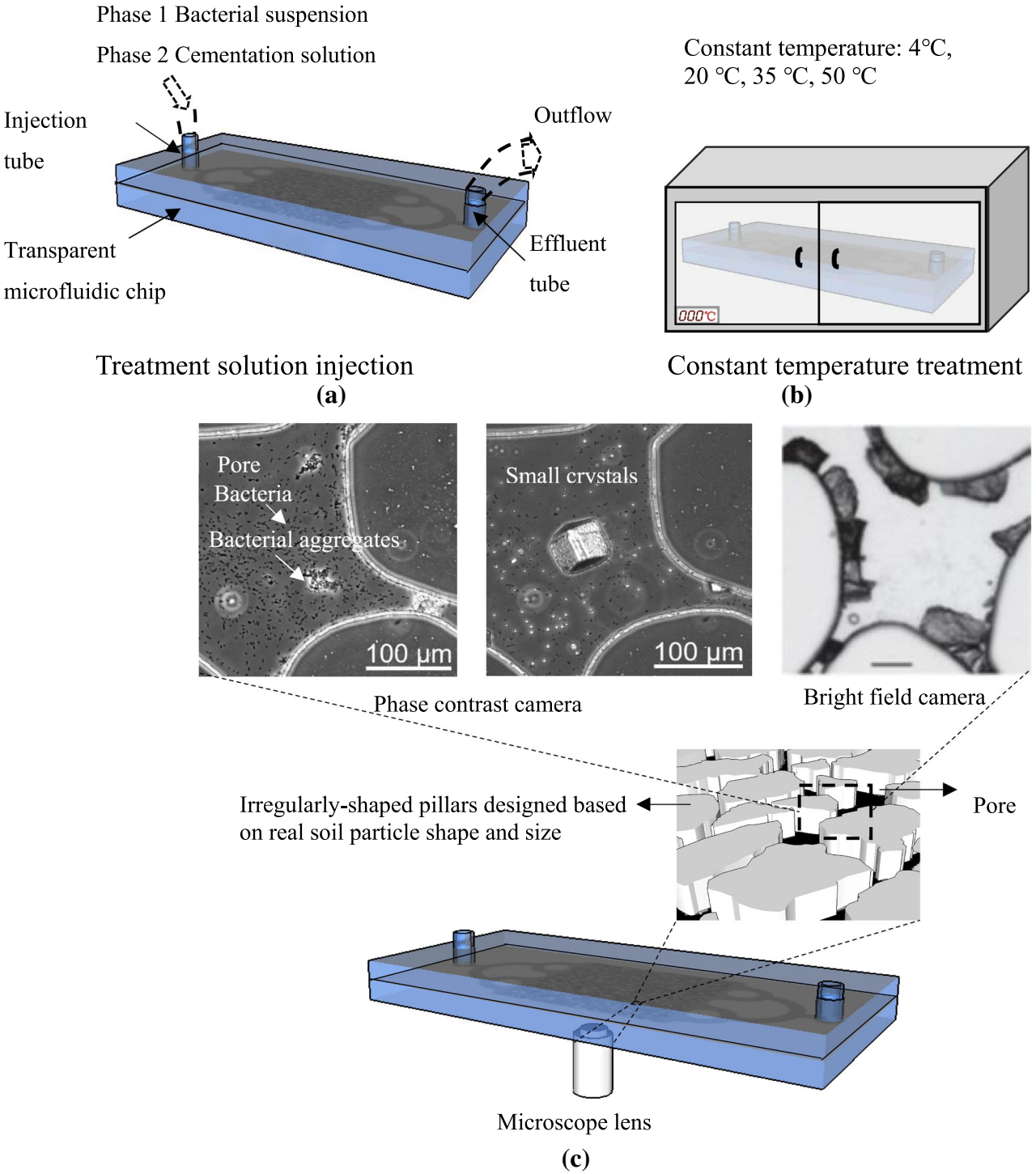

Fig. 1 Schematic of microscale microfluidic chip experiments, **a** bacterial and cementation solution injection; **b** incubation; **c** imaging

the microfluidic chip channels are usually semi-spherical and semi-rhombohedral crystals [36, 37]. To quantify the size of semi-spherical crystals, the diameters of the crystals in the 2-D images were measured by ZEN software (Zeiss) and the volumes of the half spheres were calculated. The schematics of the crystal volume calculation is shown in Fig. 2. Because the depth of the microfluidic channels is 50 μm, when the diameter of the sphere is smaller than 100 μm, the crystal volume is calculated as the volume of a half sphere:

Table 1 MICP treatment parameters for the microfluidic chip experiment

Test No	Temperature (°C)	Bacterial injection number	Bacterial settling time (h)	Cementation injection number	Injection interval of cementation solution (h)
1	4	1	18	10	48
2	20	1	18	10	48
3	35	1	18	10	48
4	50	1	18	10	48
5	50	1	2	10	6–18
6	50	5	2	10	6–18

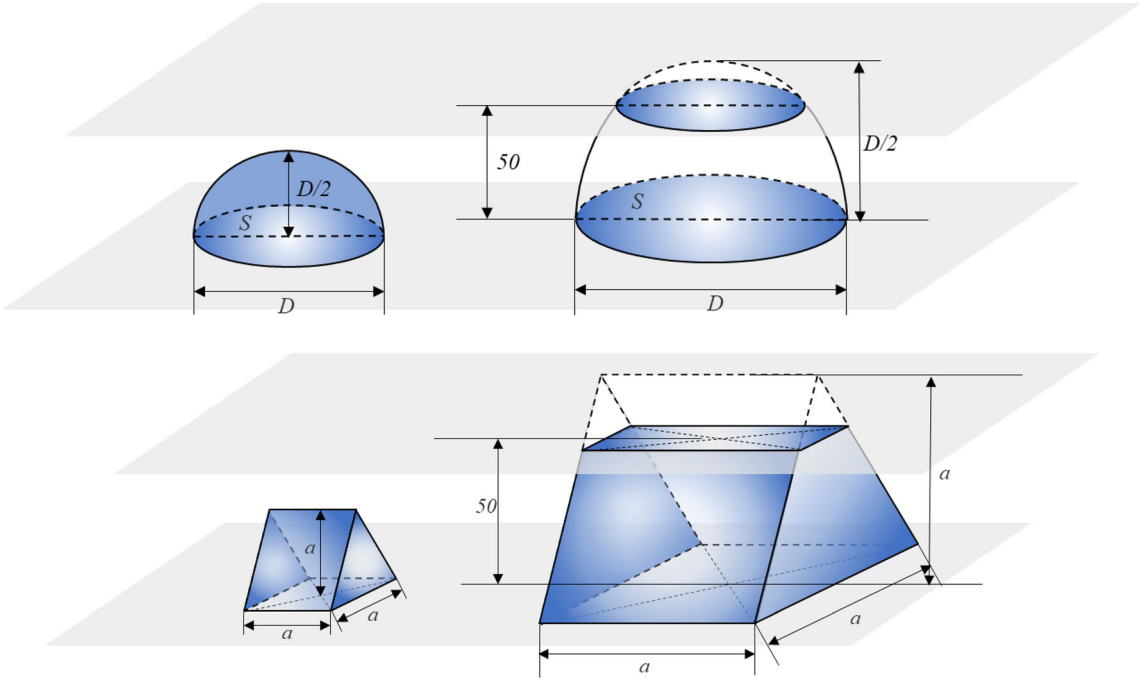

Fig. 2 Schematic of spherical and rhombohedral crystals

$$V = \frac{1}{2} \times \frac{4}{3}\pi\left(\frac{D}{2}\right)^3 = \frac{1}{12}\pi D^3 \tag{6a}$$

where D is the diameter of the half-sphere. When the diameter of the sphere is larger than 100 μm, the crystal volume is the half sphere minus volume of the cap of height, which is calculated as:

$$V = \frac{1}{12}\pi D^3 - \frac{\pi}{3}(50 + D)\left(\frac{D}{2} - 50\right)^2 \tag{6b}$$

To quantify the size of semi-rhombohedral crystals, the size of the bottom square of the crystals in the 2-D images was measured by ZEN software (Zeiss), and the height of the semi-rhombohedral crystals (denoted as a) is assumed to be the same as the length of the bottom square of the crystals. Therefore, when the height is smaller than 50 μm, the crystal volume can be calculated as:

$$V = \frac{1}{2}a^3 \tag{7a}$$

When the height of the crystal is larger than 50 μm, the crystal volume can be calculated as:

$$V = \frac{1}{2}a^3 - \frac{1}{2}(a - 50)^3 \tag{7b}$$

The number of crystals present in selected areas of the images was counted, and crystal densities were calculated by dividing the number of crystals by the volume of the pores that contain the crystals.

Chemical transformation efficiency (CTE) after the n_{th} injection of cementation solution indicates the actual mass or volume of calcium carbonate obtained after MICP

treatment relative to the theoretical calculated mass or volume of calcium carbonate obtained if all of the calcium ions injected transformed into calcium carbonate [2]. The total volume of $CaCO_3$ (assuming all crystals are calcite) is denoted as $V_{c100\%}$, the pore volume of soil samples at the beginning of MICP treatment is denoted as V_v, and the ratio of $V_{c100\%}$ relative to V_v can be calculated by [35]:

$$\left(\frac{V_{c100\%}}{V_v}\right)_n = \frac{\frac{0.5\,mol/L \times n \times 100\,g/mol \times PV}{2.71\,g/cm^3} \times 0.001\,L/cm^3}{PV} \times 100\% \quad (8a)$$

After the n_{th} injection, the total volume of $CaCO_3$ crystals as a fraction of the pore volume V_v is $(V_c/V_v)_n$. The chemical transformation efficiency after the n_{th} injections of cementation solution is:

$$(CTE)_n = \frac{\left(\frac{V_c}{V_v}\right)_n}{\left(\frac{V_{c100\%}}{V_v}\right)_n} \times 100\% = \left(\frac{V_c}{V_{c100\%}}\right)_n \times 100\% \quad (8b)$$

The individual chemical transform efficiency can be computed to determine the chemical transform efficiency after each of the injections of cementation solution. After each injection of cementation solution, if all of the injected Ca^{2+} ions fully transform into $CaCO_3$, then the total volume of calcium carbonate crystals (assuming all crystals are calcite) produced by one injection $V_{c100\%}$ relative to the pore volume V_v is:

$$\frac{V'_{c100\%}}{V_v} = \frac{\frac{0.5mol/L \times 100g/mol \times PV}{2.71g/cm^3} \times 0.001L/cm^3}{PV} \times 100\% \quad (9a)$$

As a result, the chemical transformation efficiency following an individual injection after the n_{th} injection was indicated by the volume of crystals measured after the completion of the n_{th} injection as a fraction of the pore volume V_v minus the volume of crystals measured after the completion of the $(n\text{-}1)_{th}$ injection as a fraction of the pore volume V_v:

$$(ICTE)_n = \frac{\left(\frac{V_c}{V_v}\right)_n - \left(\frac{V_c}{V_v}\right)_{n-1}}{\frac{V'_{c100\%}}{V_v}} \times 100\% \quad (9b)$$

3 Results and discussion

3.1 Effects of temperature on bacterial density and activity changes

The change in bacterial OD_{600}, ureolysis rate and specific urease activity at 4, 20, 35 and 50 °C (Tests 1–4) are shown in Fig. 3a, b and c, respectively. In all four temperature conditions, the OD_{600} values reduced with time over the 12 days, with the reduction rate being higher at higher temperatures (Fig. 3a). The reduction rate of OD_{600} is about 0.01, 0.04, 0.2 and 0.4 per day when temperature was 4, 20, 35 and 50 °C, respectively (Fig. 3a). Temperature also affects the changes of ureolysis rate (Fig. 3b). At 4 and 20 °C (Tests 1 and 2, respectively), the ureolysis rate reduced from 40 mM/h to about 25 and 30 mM/h, respectively, after about 2 days and remained almost constant until the end of the 12-day period (Fig. 3b); at 35 °C (Test 3), the ureolysis rate increased to about 60 mM/h within approximately two days and then started decreasing with time until 0 by about 12 days; at 50 °C (Test 4), the ureolysis rate reduced significantly with time to zero within just one day (Fig. 3b). To remove the effects of bacterial density on ureolysis rate, bacterial specific urease activity is plotted against time in Fig. 3c. At 4 °C, bacterial specific ureolysis rate remained almost constant at about 34 mM/h/OD_{600}; at 20 °C it increased slowly from about 35 mM/h/OD_{600} to 50 mM/h/OD_{600} within twelve days; at 35 °C, it increased linearly from about 35 mM/h/OD_{600} to about 250 mM/h/OD_{600} within 4.75 days and then reduced linearly to zero within 6.75 days; at 50 °C, it decreased linearly to zero within just one day (Fig. 3c). Figure 3d shows that temperature significantly affects the measured values of urease activity. The urease activity increased exponentially with the increase in temperature within the range from 5 to 70 °C. This result is consistent with the results of Whiffin [41] and Zhao et al. [46] and can be explained by the fact that the measured temperature has a significant influence on conductivity readings [5]. The reason for this might be that urea hydrolysis is an endothermic reaction, with an increase in temperature resulting an increased reaction rate. Therefore, according to the recommendations outlined by standard ASTM D1125-95 and the results of this experiment, in order to compare the effects of temperature on urease activity, it is essential to keep the measuring temperature the same to avoid the effects of temperature on the conductivity reading.

As inactive cells and dead cells have no contributions to MICP [45], it should be noted that in Fig. 3, the OD_{600} and ureolysis rate do not distinguish between the different effects of live and dead cells but represent the overall quantification of bacterial density and capability of ureolysis by both live and dead bacterial cells. However, as OD_{600} is a widely accepted method to quantify the total number of bacterial cells, this study shows the obvious time-dependent effects of temperature on the overall urease activity of the bacterial suspensions placed at various temperatures. Because different temperatures have different effects on the growth and death rates of bacterial cells, as well as on the ureolysis rate, future work is warranted to quantify the colony-forming unit (CFU) activity of the

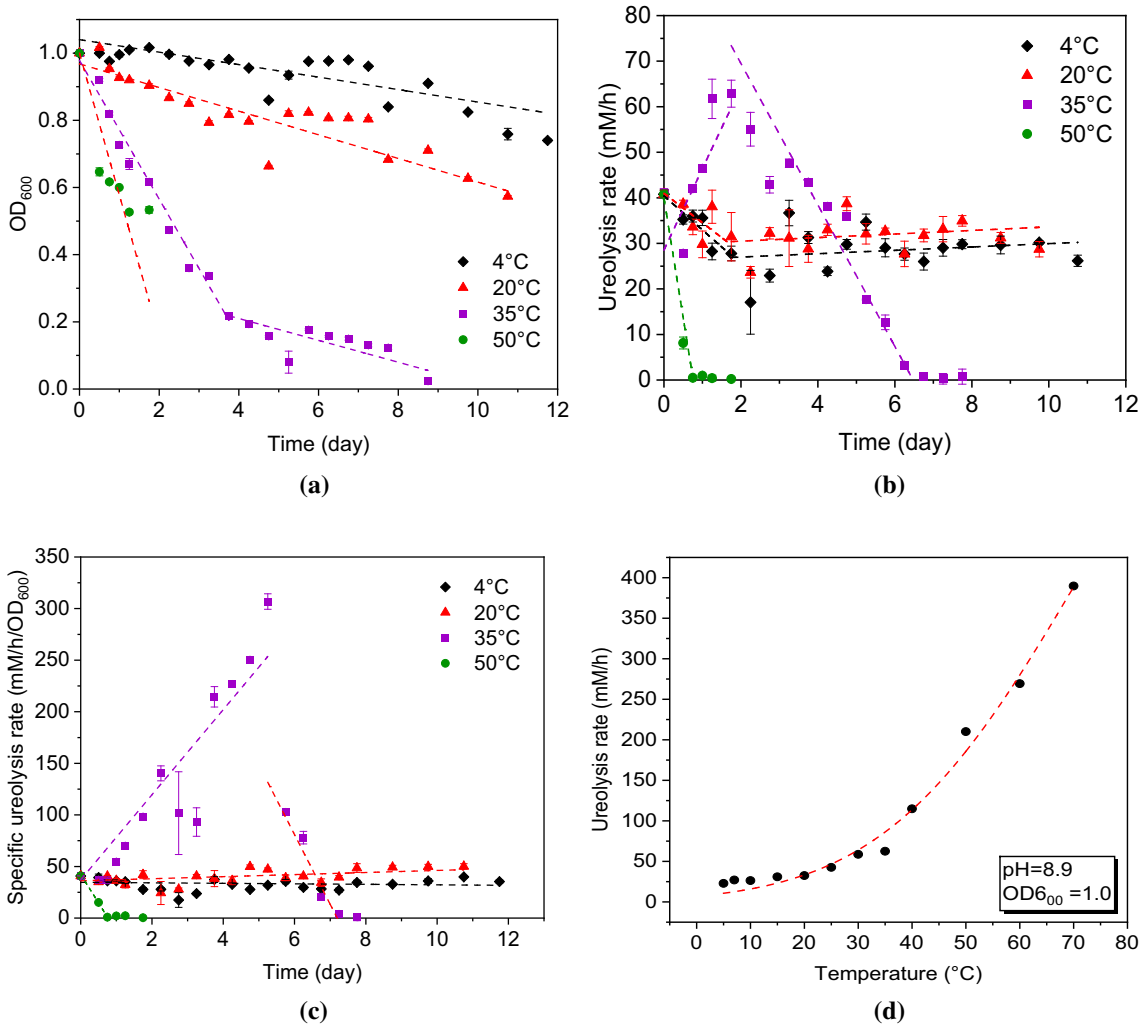

Fig. 3 Results of batch tests **a** optical density of bacterial suspension vs time; **b** ureolysis rate of bacterial suspension vs time; **c** specific ureolysis rate vs time; **d** ureolysis rate measured at varied temperatures

bacterial suspension placed at different temperatures to obtain the exact concentration of live bacterial cells and the specific urease activity contributed by the live bacterial cells.

Ureolysis rate is mainly affected by bacterial density C_B (cells/l), bacterial urease producing rate C_u (g/cells) and pure urease activity A_u (mol/l/h/g). These three parameters are all functions of temperature T and time t. The ureolysis rate can be expressed as:

$$U(T, t) = C_B(T, t) \times C_u(T, t) \times A_u(T, t) \quad (10)$$

Compared with Equations. 3, 4, 5, bacterial specific urease activity is a function of the rate of urease production and urease activity.

$$U'(T, t) = C_u(T, t) \times A_u(T, t) \quad (11)$$

The ureolysis rate can be expressed as:

$$U(T, t) = C_B(T, t) \times U'(T, t) \quad (12)$$

Bachmeier et al. [4] investigated the effects of temperature on pure free enzyme activity and found that urease activity decreases with time at different temperatures, with higher temperatures reducing the activity more quickly than lower temperatures. The percentage of remaining urease activity of the free enzyme after 1 day in their experiments was only about 90%, 60% and 10% of the original activity at temperatures of 4, 30 and 60 °C, respectively. Fathima and Jayalakshmi [16] observed that urease had maximum activity at 35 °C. Khan et al. [22] studied the urease production ability of bacterial strains at different temperatures and found that urease production rates increase with temperature until the temperature reached 35 °C, after which urease activity started decreasing until 50 °C.

In this study, the reduction in ureolysis rate at 4 °C (Test 1, Fig. 3b) was mainly caused by bacterial density C_B which reduced with time (Fig. 3a), but was unaffected by

bacterial specific urease activity U' which remained constant over the 12-day period (Fig. 3c). The ureolysis rate was higher at 20 °C (Test 2) than at 4 °C (Fig. 3b). This is because, although the bacterial density decreased by a greater extent at 20 °C than at 4 °C (Fig. 3a), the increase in U' at 20 °C compensated for the decrease in urease activity. According to the study of Khan et al. [22], the increase in U' might be due to the higher urease production rate at 20 °C than at 4 °C. At 35 °C (Test 3), even though the optical density of bacterial suspension reduced to a greater extent with time than at 20 °C or 4 °C (Fig. 3a), ureolysis rate still increased with time during the first two days (Fig. 3b). This is because an increase in bacterial specific urease activity compensated for a decrease in bacterial density (Fig. 3a and c). However, after two days, urease activity at 35 °C reduced with time and this is because the increase in bacterial specific urease activity could not compensate for the decrease in bacterial density (Fig. 3a and c). At 50 °C (Test 4), the reduction in bacterial urease activity with time (Fig. 3b) was due to the reduction in both bacterial density (Fig. 3a) and bacterial specific urease activity (Fig. 3c) with time.

3.2 Effects of temperature on bacterial growth and attachment

The effects of temperature on bacterial growth and attachment were investigated using microfluidic chip experiments. The microscope images are shown in Fig. 4a and the quantification results are shown in Fig. 4b. Although the bacterial density after injection was similar (see the first row of Fig. 4a and the white columns of Fig. 4b), the bacterial density after the injections of cementation solution varied (see the third row of Fig. 4a and the dark grey columns of Fig. 4b). This is due to both the difference in amount of in situ bacterial growth, and the difference in bacterial detachment by the injection of cementation solution. As shown by the differences between the first row and the second row in Fig. 4a and between the white and light grey columns in Fig. 4b, optimal growth of bacteria was observed when the temperature was 20 °C (Test 2). In addition, as shown by the differences between the second row and the third row in Fig. 4a and between the light grey and dark grey columns in Fig. 4b), optimal attachment of bacteria was observed when the temperature was 35 °C (Test 3). It should be noted that because the duration of injection of cementation is about ten minutes, which is relatively short, bacterial growth during the injection of cementation solution can be neglected. The factors affecting bacterial attachment to a solid substrate are complex. Previous research has shown that bacteria tend to secrete structures such as flagella, pili, exopolysaccharides and other matrix components to attach

Fig. 4 **a** Microscope images of a middle pore of the microfluidic chips taken after bacterial injection (*), after bacterial settling (**) and after cementation solution injection (***); **b** the quantification of the bacterial densities in images shown in **a**

to solid surfaces and live at the solid–liquid interface [14]. In addition, bacterial cells and soil particles are in general negatively charged, therefore, Ca^{2+} in the cementation solution can increase the aggregation among bacterial cells [37] and bacterial attachment to the soil substrate. Further, higher concentration of cementation solution hindered the diffusion of bacterial cells into cementation solution [44], which may further increase the attachment of bacterial cells to the substrate. This study illustrated that apart from the concentration of $CaCl_2$ in the cementation solution, temperature also affects the attachment of bacteria to the substrate. The reason that temperature affects bacterial attachment may be due to the temperature effects on bacterial secretion behavior, surface charges, motility, etc., which is worthy of further exploration in future studies.

After the injections of cementation solution, the highest bacterial density was obtained when the temperature was 35 °C, while the lowest bacterial density was obtained when temperature was 4 °C. The bacterial densities were about 0.3, 3, 3.5 and 1.1 times of their initial values for the temperature conditions of 4, 20, 35 and 50 °C, respectively. Therefore, when considering the effects of bacterial growth, the bacterial density C_B in Eq. 9 is a function of temperature, time, nutrient /oxygen condition, flow rate, solid surfaces conditions, etc.

3.3 Temperature-dependent crystal growth procedure after the 1st and 2nd injections

Microscopic images of one pore in the central region of the microfluidic chips at 3, 6, 24 and 48 h after the first and second injections of cementation solution are shown in Fig. 5 for the four temperature conditions (4, 20, 35 and 50 °C, Tests 1–4). Chemical transformation efficiencies, crystal number and crystal precipitation rates of crystals shown in Fig. 5 were quantified, and the results are shown in Fig. 6 a, b and c. It can be seen from Figs. 5 and 6a that crystals grow more slowly at 4 °C compared to the other three temperature cases. For the temperature cases of 20 °C, 35 °C and 50 °C, after the first injection of cementation solution, crystals completed precipitation within 6 h, whereas for the 4 °C case crystals did not complete their precipitation by 48 h. In addition, the crystal growth rates after the first injection of cementation solution were also different to those after the second injection, especially at 50 °C, where the time for the crystals to complete the precipitation after the first and second

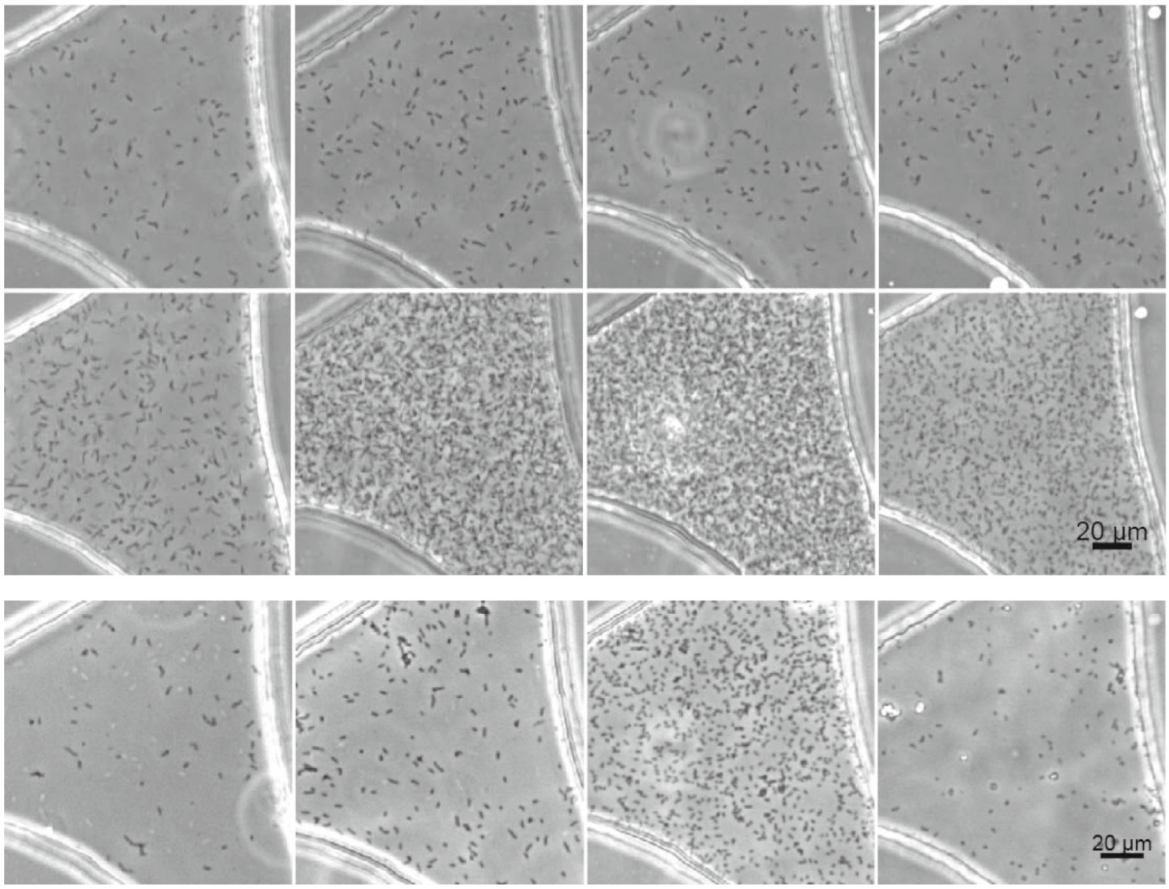
*
**
***
20 μm
20 μm
4°C
20°C
35°C
50°C

(a)

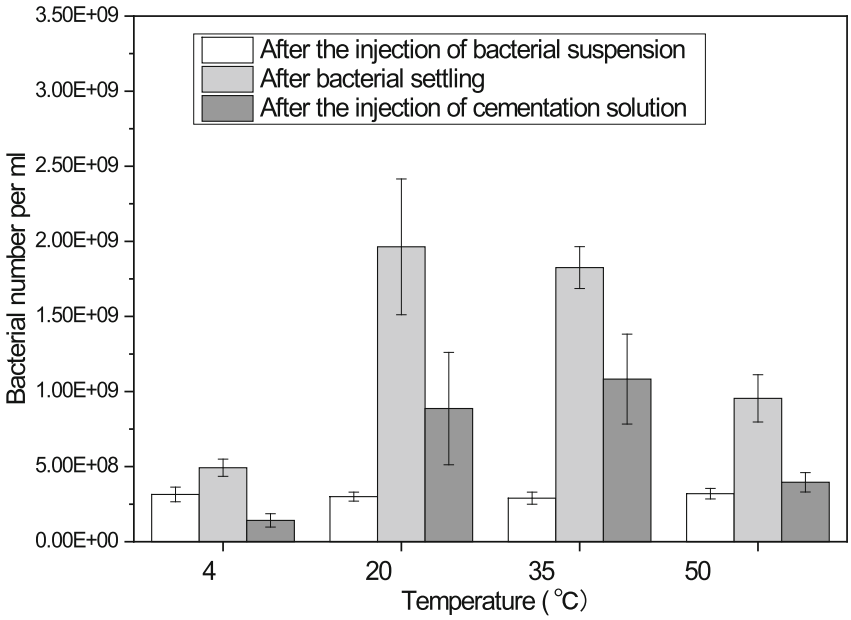
After the injection of bacterial suspension
After bacterial settling
After the injection of cementation solution
Bacterial number per ml
3.50E+09
3.00E+09
2.50E+09
2.00E+09
1.50E+09
1.00E+09
5.00E+08
0.00E+00
4
20
35
50
Temperature (℃)

(b)

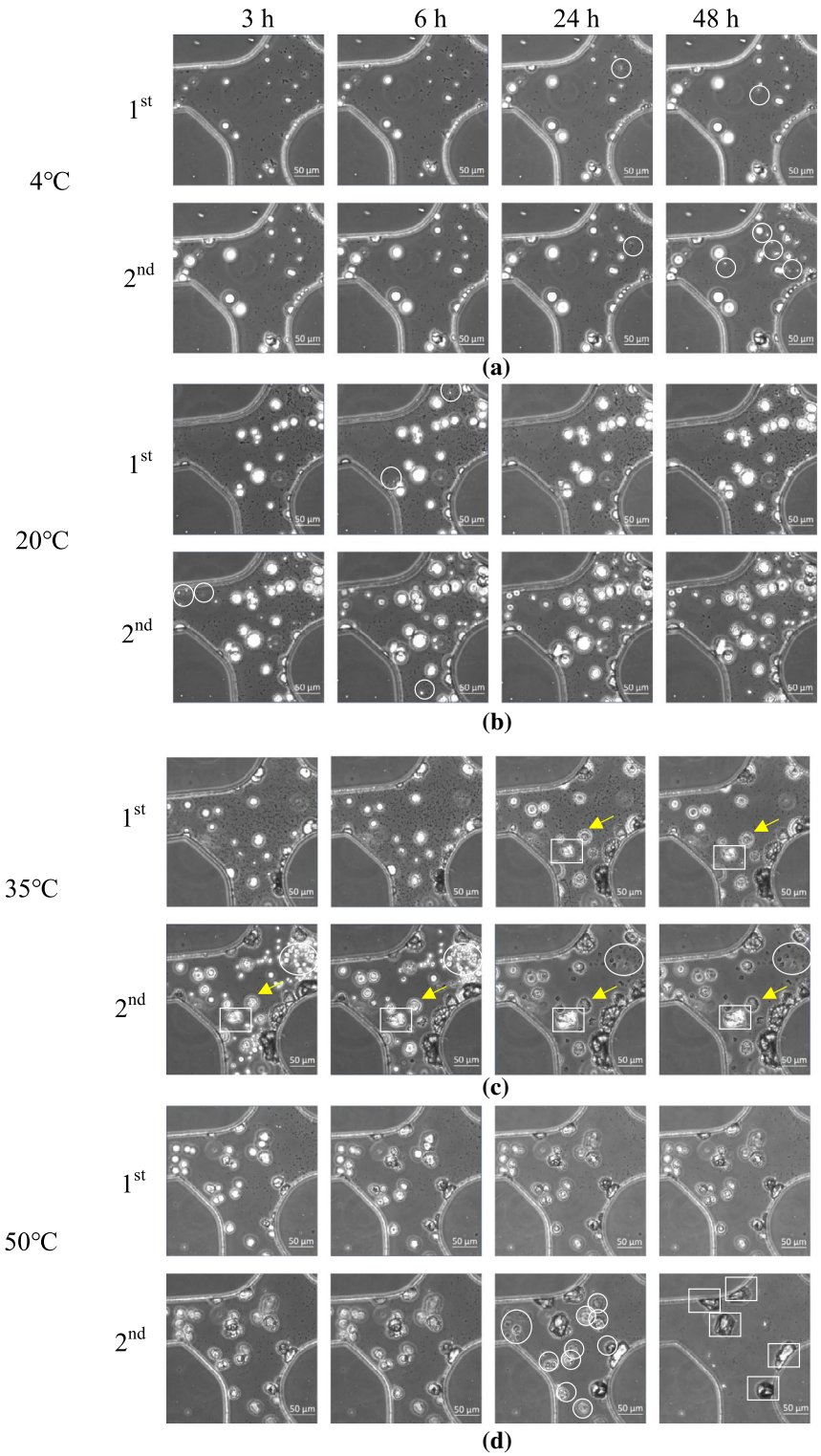

Fig. 5 Sequential microscope images taken on one pore at the central region of the microfluidic chips placed at 4, 20, 35 and 50 at 3, 6, 24 and 48 h after the first and second injection of cementation solution, **a** 4 °C, **b** 20 °C, **c** 35 °C and **d** 50 °C

injections of cementation solution was 6 and 48 h, respectively. Moreover, the growth rate at 20 °C is consistent with the results of Wang et al. [36], wherein for a cementation solution of concentration 0.25 M, the time for crystals to fully precipitate is about 3 h. In the present study, the concentration of cementation solution is doubled and hence the time required to precipitate doubled as well.

It can be seen from Figs. 5 and 6b that crystal number increases due to the growth of new crystals and decreases due to the dissolution of unstable crystals. At 4 and 20 °C, crystal number mainly increases after the first two injections of cementation solution. However, at 35 °C and 50 °C, a crystal precipitation–dissolution–reprecipitation process was observed, as shown by the white circles in the second rows of Fig. 5c and d. With the dissolution of unstable crystals, the crystal number also reduced (Fig. 5b). In addition, the dissolution mainly occurred between 6 and 24 h after the first two injections of cementation solution at 35 °C and after the second injections of cementation solution at 50 °C (Figs. 5c, d and 6b).

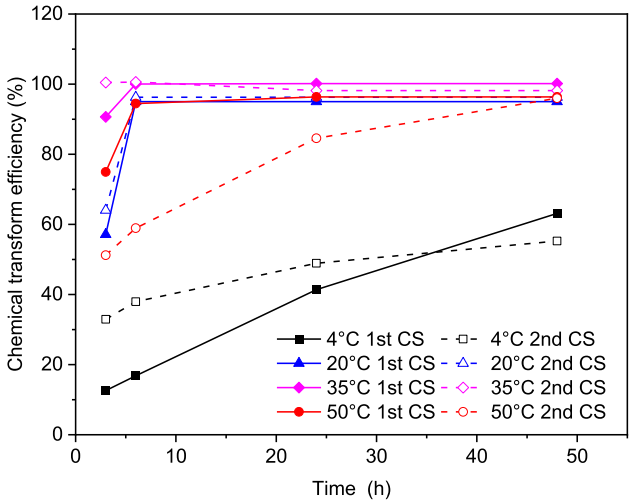

(a)

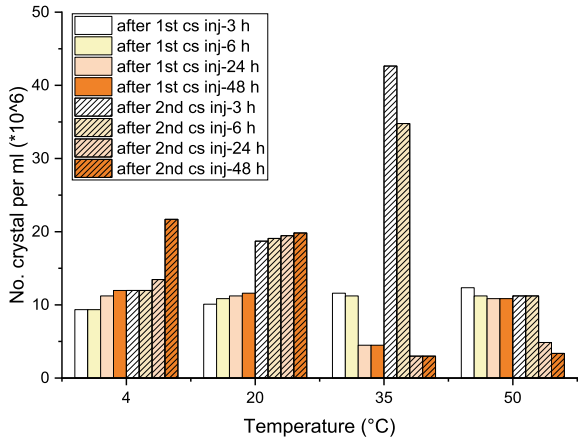

(b)

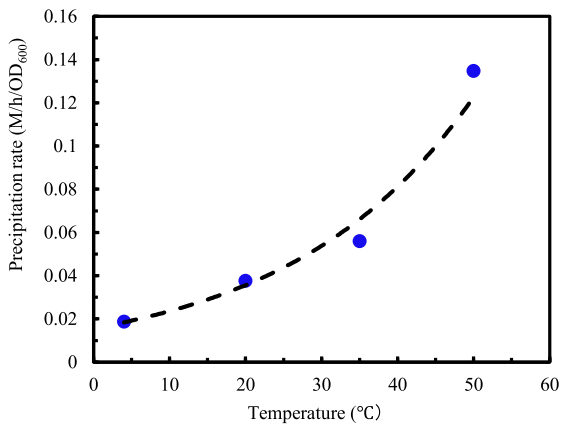

(c)

Fig. 6 Quantification results of images shown in Fig. 5. **a** chemical transform efficiency; **b** crystal number; **c** precipitation rate

The precipitation-dissolution-reprecipitation process of these crystals is consistent with Ostwald's law of crystal ripening; usually, the least dense phase is formed first and transforms to the next dense phase until finally the densest (which is usually also the most stable phase) is formed (reviewed by [11]. The shapes and stabilities of the spherical and rhombohedral $CaCO_3$ crystals are consistent with those of vaterite and calcite, respectively, which is consistent with the previous studies of Wang et al. (2019b, 2021. Calcite is the most stable form of $CaCO_3$ crystals. In addition, the dissolved crystals have a 'memory-like' effect; that is, when a new batch of cementation solution is injected, the crystals tend to reprecipitate where the crystals used to be located after the previous injection before they dissolved (see the changes of the crystal indicated by the yellow arrows in Fig. 5c). This is probably because the crystals did not fully dissolve, with some crystal lattice still remains on the channel surface of the porous medium. Crystals grow on existing lattices because less energy is required than growing on a new surface due to the extra energy required for nucleation [24].

At 4 °C, the chemical transformation efficiencies were around 64% by 48 h after the first injection of cementation solution (Fig. 6a). Based on this rate an injection interval of approximately 75 h is required to achieve a high chemical transform efficiency (about 100%). In addition, based on the chemical transform efficiency at 3 h in the 20 °C (Test 2), 35 °C (Test 3) or 50 °C (Test 4) cases (Fig. 6a), the time required for 0.5 M of cementation solution to complete precipitation after the first injection of cementation solution is 6, 3.3 or 3.75 h, respectively. Considering the difference in bacterial density after the injections of cementation solution in these four cases (shown in Fig. 3b) and given that the bacterial suspension has 4×10^8 cells per ml when OD_{600} is 1.0 based on results of Wang et al. [37], the calculated precipitation rates in these four conditions are 0.018, 0.038, 0.056 and 0.135 M/h/OD, respectively (Fig. 6c). As the temperature increases, crystal growth rate increases exponentially (Fig. 6c).

3.4 Temperature-dependent crystal growth procedure after the 2nd to 10th injections

To observe the crystal growth during the entire treatment process, microscope images of one pore located near the center of the microfluidic chip were taken two days after the injections of the second, fourth, sixth, eighth and tenth injections of cementation solution and are shown in Fig. 7. The quantified average crystal volume, crystal number per unit pore volume, ratio of crystal volume to pore volume ($V_{crystals}/V_{pore}$), total chemical transformation efficiency and individual chemical transformation efficiency are given in Fig. 8a–e.

The average crystal volume for the three cases grew steadily as the number of cementation solution injections was increased (Figs. 7 and 8a), except for the 50 °C case (Test 4) where individual crystals stopped growing after the fourth injection of cementations solution. At 4, 20, 35 °C and 50 °C (Tests 1–4), the average crystal size increased at rates of 402.4, 1344.3, 1881.8 and 312.5 μm^3 per injection, respectively. After the completion of the tenth treatment, the average crystal size was the largest when the temperature was 35 °C (Test 3), and the smallest when the temperature was 4 °C (Test 1, Figs. 7 and 8a).

Crystal number can increase due to the precipitation of new crystals and decrease due to the dissolution of unstable crystals (Figs. 5 and 7). At 4 °C (Test 1), crystal number remained constant (Fig. 5), possibly because this low temperature does not provide enough energy for new crystals to nucleate, and because dissolution of crystals does not occur. At 20 °C (Test 2), the number of crystals decreased with time, indicating that dissolution of crystals occurred at 20 °C, but the dissolution rate was lower than at 35 °C (Test 3) and 50 °C (Test 4), shown by the much higher crystal number at 20 °C than at 35 °C or 50 °C (Fig. 8b). At 35 °C, the dissolution procedure completed within the 48 h after each injection and the growth of new crystals appeared constant after each injection (Figs. 7 and 8b). At 50 °C, crystals continued growing during the first two injections of cementation solution (Fig. 6), but stopped growing after the fourth injection of cementation solution (Figs. 7 and 8). In addition, the dissolution procedure at 50 °C completed within 48 h after the first injection of cementation solution (Figs. 6 and 8b); therefore, the number of crystals remained constant (Fig. 8b). Even though the crystal number remained the same at both 4 °C and 50 °C, the number of crystals observed at 4 °C was much higher than at high temperature because crystal dissolution occurred at 50 °C but not at 4 °C (Fig. 8b).

The total crystal volume is indicated by the volume ratio of crystal volume to pore volume and is plotted against the measured crystals number in Fig. 8c. At 4, 20 and 35 °C crystals grew steadily at almost constant rates, indicated by the ratio of total crystal volume to pore volume (Fig. 8c), with the highest rate being observed at 20 °C, while the lowest rate was observed at 4 °C. At 50 °C, crystals stopped growing after the fourth injection of cementation solution (Fig. 8c), and the growth rates after the first four injections of cementation solution are similar to those at 4 °C.

At these four temperatures, the total chemical transform efficiency varied significantly and decreased linearly with time at different rates. The initial chemical transform efficiencies obtained at 35 °C and 20 °C were about 100% and 90%, respectively. They were much higher than the initial chemical transformation efficiencies at 50 °C and 4 °C, which were about 60% and 50%, respectively. However, due to the difference in reduction rate of chemical transformation efficiency with time, at 4, 20, 35 and 50 °C, the chemical transformation efficiencies after the 10th injection were about 30%, 80%, 70% and 30%, respectively (Fig. 8d). The individual chemical transformation efficiencies decreased at similar rates when the temperatures were 4 °C and 20 °C (about 4% per injection), but reduced much more quickly when the temperature was 35 °C. The efficiency reduced even more quickly when the temperature was 50 °C where the transformation efficiency reduced to zero by the 6th injection of cementation solution (Fig. 8e).

In summary, temperature has both a direct effect and indirect effect on crystal growth rate. The direct effect occurs when the supersaturation ratio is the same, with an increase in temperature leading to an increase in the $CaCO_3$ precipitation rate. The indirect effect is that temperature affects the bacteria quantity and activity, which in turn affects the rate of carbonate production, and consequently affects the supersaturation condition. For example, the crystal growth rate is higher at 4 °C than at 50 °C. Although the number of bacteria remaining after the injection of cementation solution is higher at 50 °C than at 4 °C and $CaCO_3$ crystal growth rate is usually higher at higher temperatures when the supersaturate ratio is the same, the specific urease activity at 50 °C decreases significantly with time and reduces to zero after a relatively very short period of time. At 4 °C, however, the urease activity remains constant at a relatively high rate. The same reason is valid for the comparison between the 35 °C case and the 20 °C case. At 35 °C, the bacterial density is higher than that at 20 °C, but because at 35 °C the urease activity increases to peak and then reduces with time, the MICP rate and efficiency are lower than those at 20 °C.

Han et al. [20] found that $CaCO_3$ content obtained at 50 °C is higher than the $CaCO_3$ content obtained at 35 °C. This is contrary to the results herein, where after 10 injections of cementation solution the $CaCO_3$ content

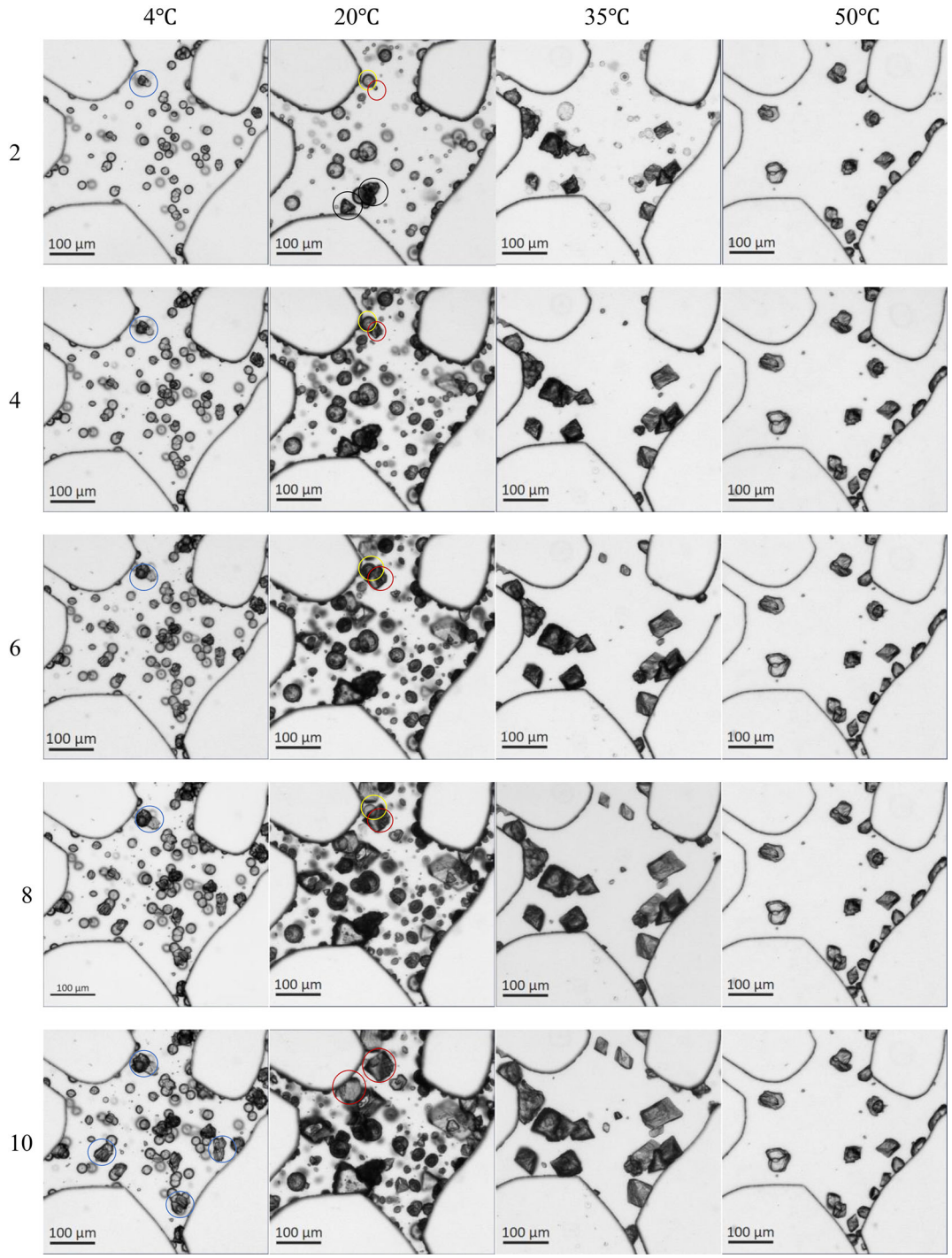

Fig. 7 Microscope images taken on one pore at the central region of the microfluidic chips placed at 4, 20, 35 and 50 °C at two days after the 2nd, 4th, 6th, 8th and 10th injections of cementation solution

obtained at 35 °C is much higher than the $CaCO_3$ content obtained at 50 °C. The reason might be that a 18-h bacterial settling time was set in this study, over which the urease activity decreased significantly at 50 °C, but increased at 35 °C. Therefore, when the cementing solution was introduced into the system after settling, 50 °C resulted in low precipitation and 35 °C resulted in high precipitation. However, in the study of Han et al. [20], there was not a settling time defined. Therefore, bacterial setting time might be an important factor to consider for MICP

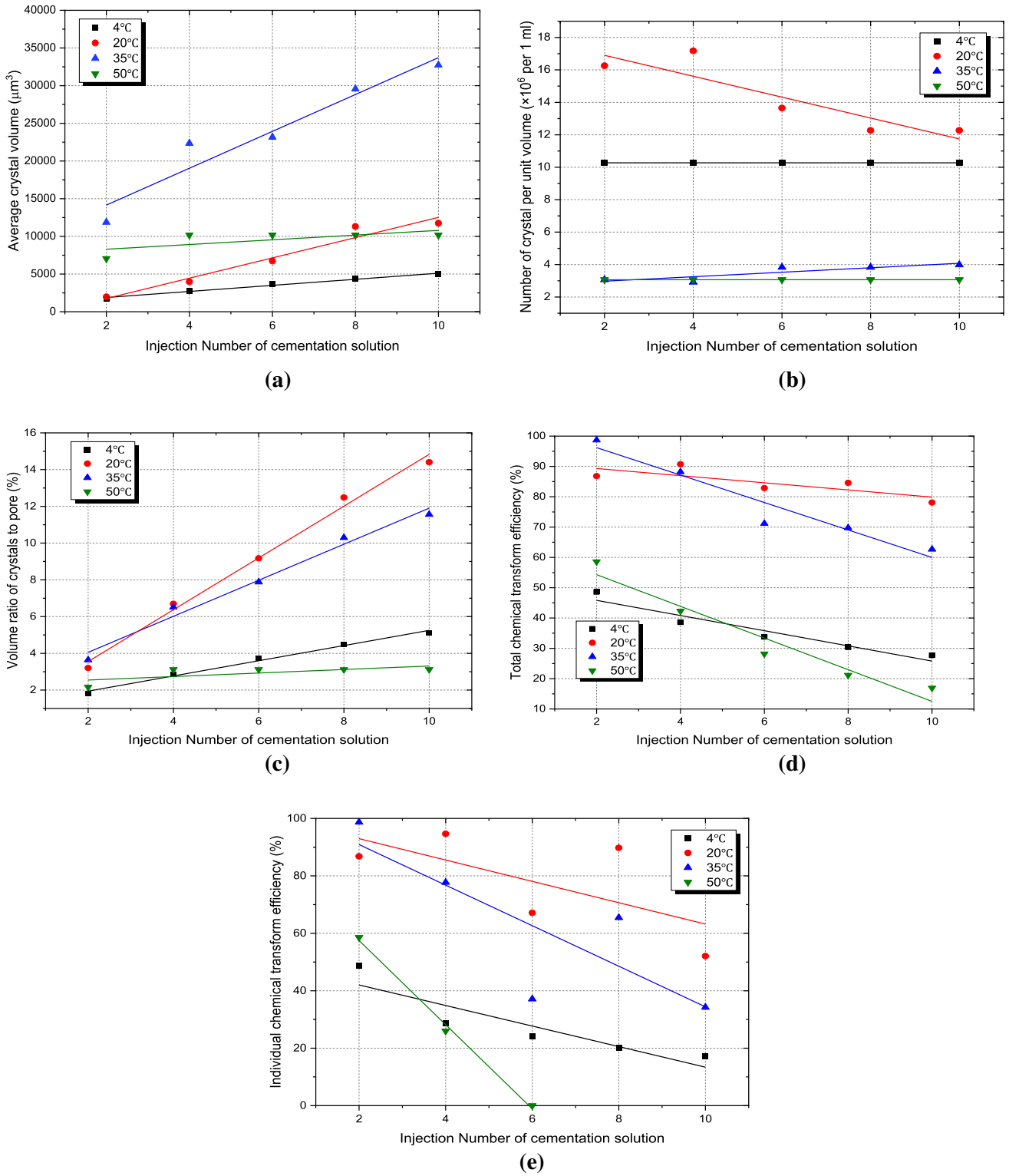

Fig. 8 Quantification results of Fig. 7 **a** Average crystal volume vs injection number of cementation solution; **b** number of crystals per unit pore volume vs injection number of cementation solution; **c** total crystal volume/pore volume vs injection number of cementation solution; **d** chemical transform efficiency vs injection number of cementation solution; **e** Individual chemical transform efficiency vs injection number of cementation solution

studies, especially when urease activity changes over the settling hours. The results of the microfluidic chip experiment where $CaCO_3$ stopped growing after the fourth day (Figs. 7 and 8b) is slightly different to the results of the batch bacterial activity experiment where the bacterial activity reduced to zero by the end of the first day (Fig. 3b and c). This might be because in the microfluidic chip experiment new injections of cementation solution containing nutrient broth were injected into the microfluidic channel every two days, with the nutrient broth increasing the bacterial activity. However, the results of the microfluidic chip experiment still show that compared to the other temperature conditions, a high temperature of 50 °C significantly reduced crystal precipitation.

3.5 Effects of temperature on crystal dissolution

To observe the crystal dissolution in detail, the images of the center pores at 4, 20, 35 and 50 °C (Tests 1–4) at two days after the 1st, 2nd, 4th, 6th, 8th and 10th injections of cementation solution are shown in Fig. 9. The crystals that used to exist at some point but dissolved at later stages are circled in red. Dissolution occurred at temperatures of 20, 35 and 50 °C, but not at 4 °C. At 20 °C, some of the crystals dissolved between the 4th and 6th injections (shown by the red circles in the 4th injection image) and between the 6th and 10th injection (shown by blue arrows where the crystal color became lighter indicating crystal dissolution). At 35 °C and 50 °C, the crystals dissolved between the first and the second injections, but not afterward. This result is the same as shown in Fig. 8b. After the 2nd, 4th, 6th, 8th and 10th injections of cementation solution, the number of crystals decreased gradually at 20 °C, whereas the number of crystals remained almost constant at 35 °C and 50 °C.

To observe a larger area, the images of a 1.5 mm by 1.5 mm square area taken at the middle of the microfluidic chip at 2 days after the first and tenth injection of cementation solution are shown in Fig. 10. Crystal dissolution occurred at 20 °C, 35 °C and 50 °C (Tests 2–4), but not at 4 °C (Test 1). In addition, a rise in temperature promoted crystal dissolution as shown by the increase in numbers of red circles from 4 to 50 °C. This trend is consistent with the results of Kralj et al. [24] where a pure chemical precipitation of $CaCO_3$ and transformation from vaterite to calcite at, 25, 35, 40 and 45 °C were studied.

3.6 Effects of temperature on crystal characteristics

To observe crystal characteristics, microscope images taken at the center of the microfluidic chips at the completion of the MICP treatments at these four temperature conditions are shown in Fig. 11. The magnified images of four pores presented in Fig. 11 are shown in Fig. 12 to examine the details. Figure 11 shows that the crystals were in general homogenously distributed within the field of view with a size of 2.5 mm by 2.5 mm. The homogenous distribution within the entire field of view is consistent with the previous published studies by Wang et al. (2019a, b). In addition, Xiao et al. [43] found that diffusion of cementation solution facilitates the uniform distribution of calcium carbonate precipitates. It is shown in Fig. 12 that crystals were mainly spherical at 4 °C (Test 1), appeared as a mixture of spherical and rhombohedron crystals at 20 °C (Test 2), while rhombohedral calcite crystals were observed at 35 °C (Test 3) and 50 °C (Test 4). The number of rhombohedral crystals and all crystals shown in the images of Fig. 11 was counted manually, and the ratio of the number of rhombohedral crystals to the total number of crystals was about 20%, 35%, 100% and 100% at 4 °C, 20 °C, 35 °C and 50 °C, respectively. The existence of mixtures of rhombohedral and spherical crystals, and the transformation of spherical crystals into rhombohedral crystals at 20 °C is consistent with previous results published by Wang et al. (2019a, b), Xiao et al. [43]. The rhombohedral rystal shape is consistent with the morphology of calcite, whereas spherical crystals were identified as vaterite [10] or the transforms of calcite from vaterite [43]. This suggests that high-temperature conditions favored the formation of calcite and the transformation of vaterite into calcite, whereas low-temperature conditions favored the formation of vaterite.

3.7 Optimization of MICP treatment procedures based on the findings

This study has shown that, at high temperatures such as 50 °C (Test 4), crystal growth rate should be high if the bacterial density and urease activity are constant (Fig. 6c). However, due to the effects of high temperature on the reduction of both bacterial density and bacterial specific urease activity (Fig. 4a, c), the amount of $CaCO_3$ precipitated and chemical transformation efficiency of MICP were even lower than at 4 °C (Fig. 8 c, d). At 50 °C, bacterial density and specific urease activity both decreased very quickly with time (Test 4, Fig. 3a, c). Because crystals almost completed the precipitation by 6 h after the first injection at 50 °C (Test 4, Fig. 6a), it is considered that reducing the injection interval from 48 h to 6–18 h (Test 5) and increasing bacterial injection number (Test 6) would increase the chemical transform efficiency of MICP at 50 °C. The results in Fig. 13 a, b show that reducing the injection interval to 6–18 h from 48 h helped to increase the total volume of crystals precipitated after the first two injections, but not afterward. The total crystal volume after

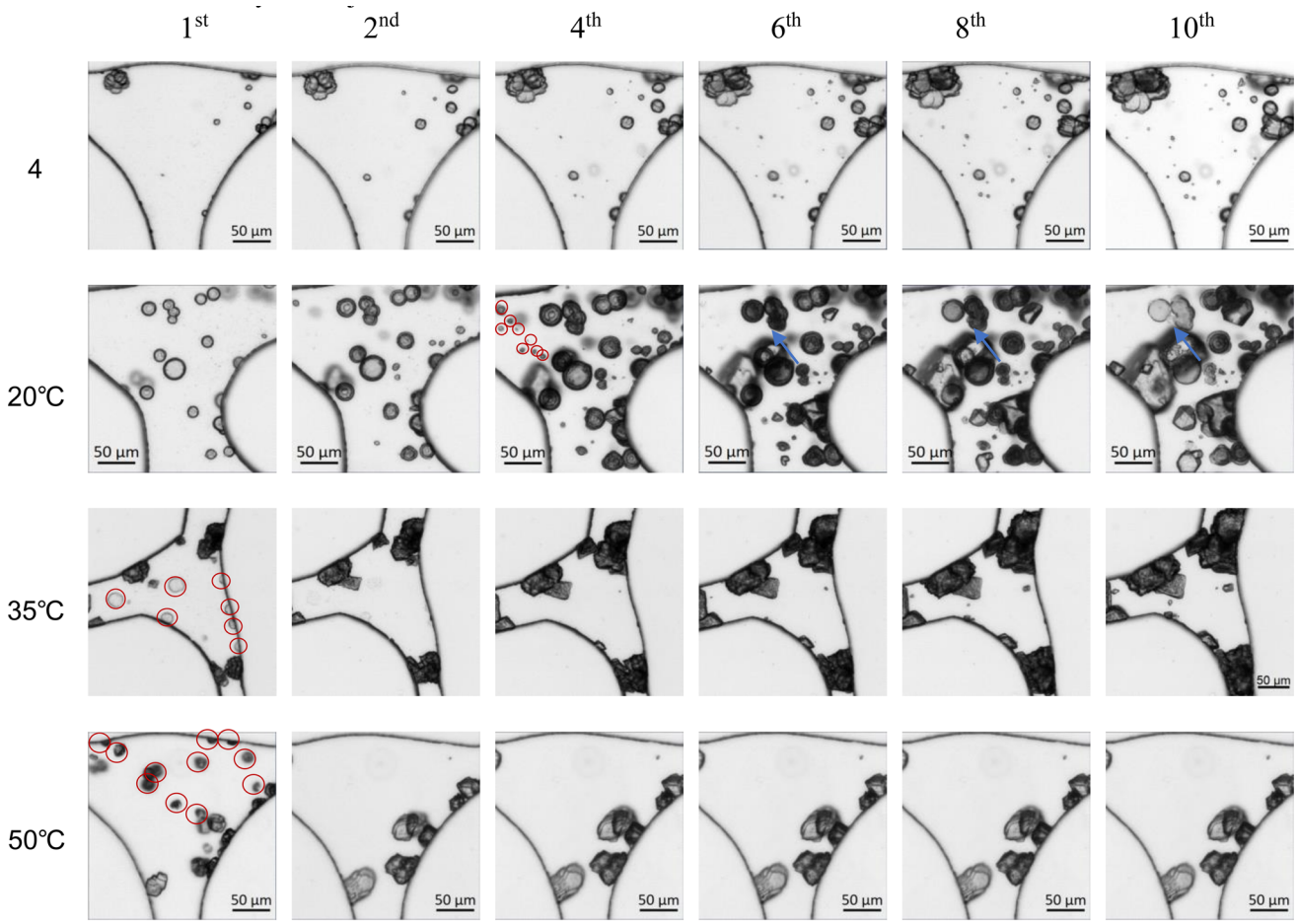

Fig. 9 Microscope images at two days after the 1st, 2nd, 4th, 6th, 8th and 10th injections of cementation solution

the fourth injection of cementation solution was higher in the case where additional injections of bacterial suspension were applied than in the other two cases, with $V_{crystals}/V_{pore}$ increasing linearly with each subsequent injection at a rate about 2.8%, per two injections (Fig. 13b). The chemical transformation efficiency remained relatively high in the case where additional injections of bacterial suspension were applied, which is about 70% over the course of the ten injections, whereas for the other two cases, the chemical transformation efficiency decreased after each subsequent injection (Fig. 13c). Figure 14 shows the images of the three cases at a larger scale (Fig. 14a) and with more pores being shown (Fig. 14b). The crystal precipitation patterns and characteristics are consistent with the images shown in Fig. 13.

This study also found that the crystal growth rate is also low at a low temperature of 4 °C. The reason for this is mainly because the precipitation rate of $CaCO_3$ is lower at lower temperatures (Fig. 6a). Wang et al. [37] found that, when temperature is constant, increasing bacterial density helped to increase the number of $CaCO_3$ crystal precipitated, but it did not affect the growth rate of the individual crystals. Therefore, higher bacterial density increases the total precipitation rate. Because the in situ growth and attachment of bacteria at 4 °C is relatively low (Fig. 3), increasing the density of bacterial suspension injected would increase the precipitation rate of $CaCO_3$. However, Wang et al. [37] found that, when bacterial density is higher, larger number of smaller crystals can be produced and the crystal dissolution-reprecipitation process takes longer. In this study, the bacterial density in the microfluidic chip at 4 °C is lower than that at 20 °C or 35 °C, but the number of crystals is still much higher (Fig. 8b). This is possible because lower temperature impairs the crystal phase transformation process (Fig. 9 and 10). Based on the findings of Wang et al. [37] and this study, the application of a higher bacterial density would increase the

Fig. 10 1500 µm by 1500 µm sized microscope images taken at the middle of the microfluidic chips at 2 days after the 1st and 10th injections of cementation solution ▶

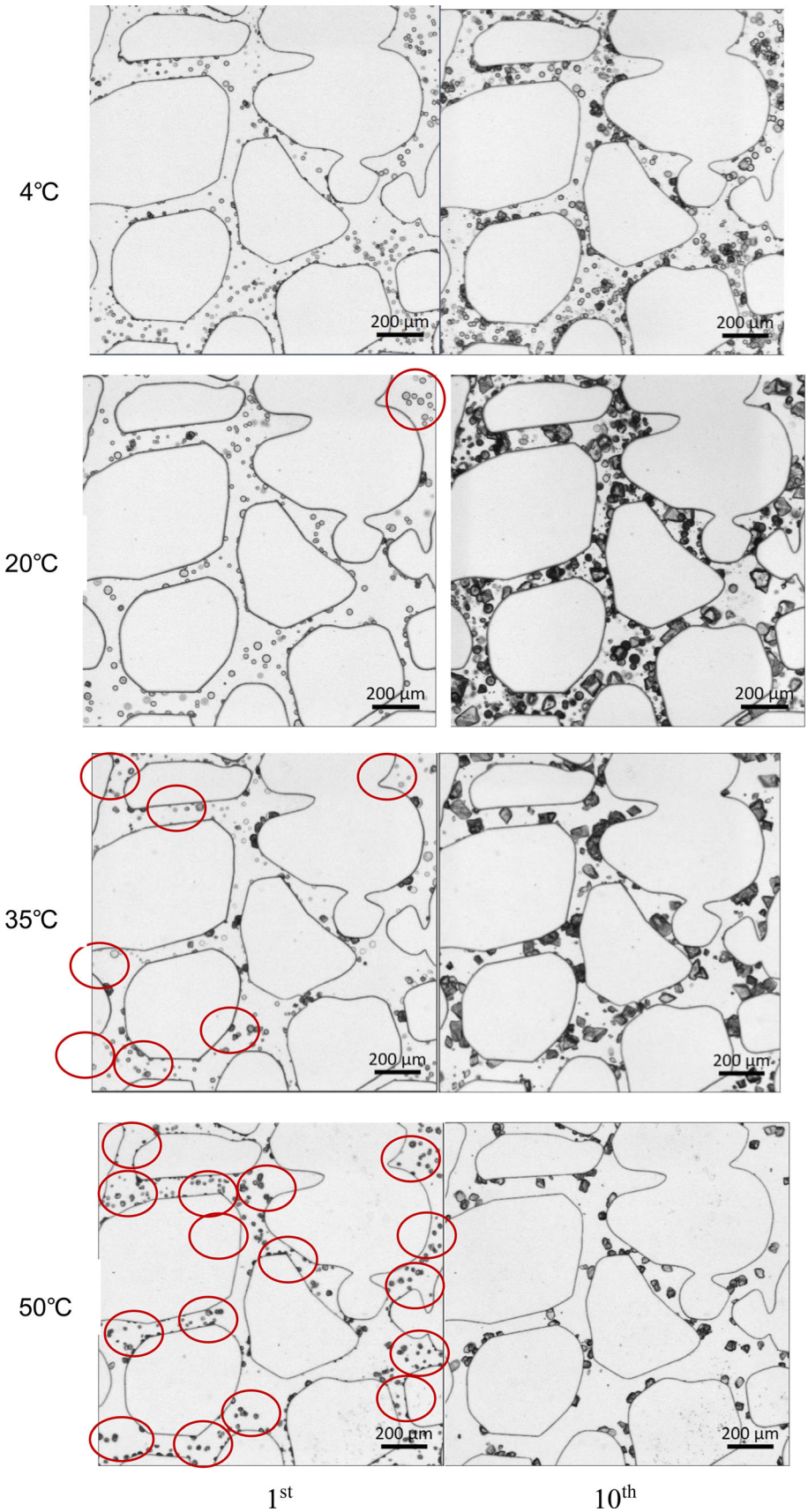
4°C
20°C
35°C
50°C
200 µm
1st
10th

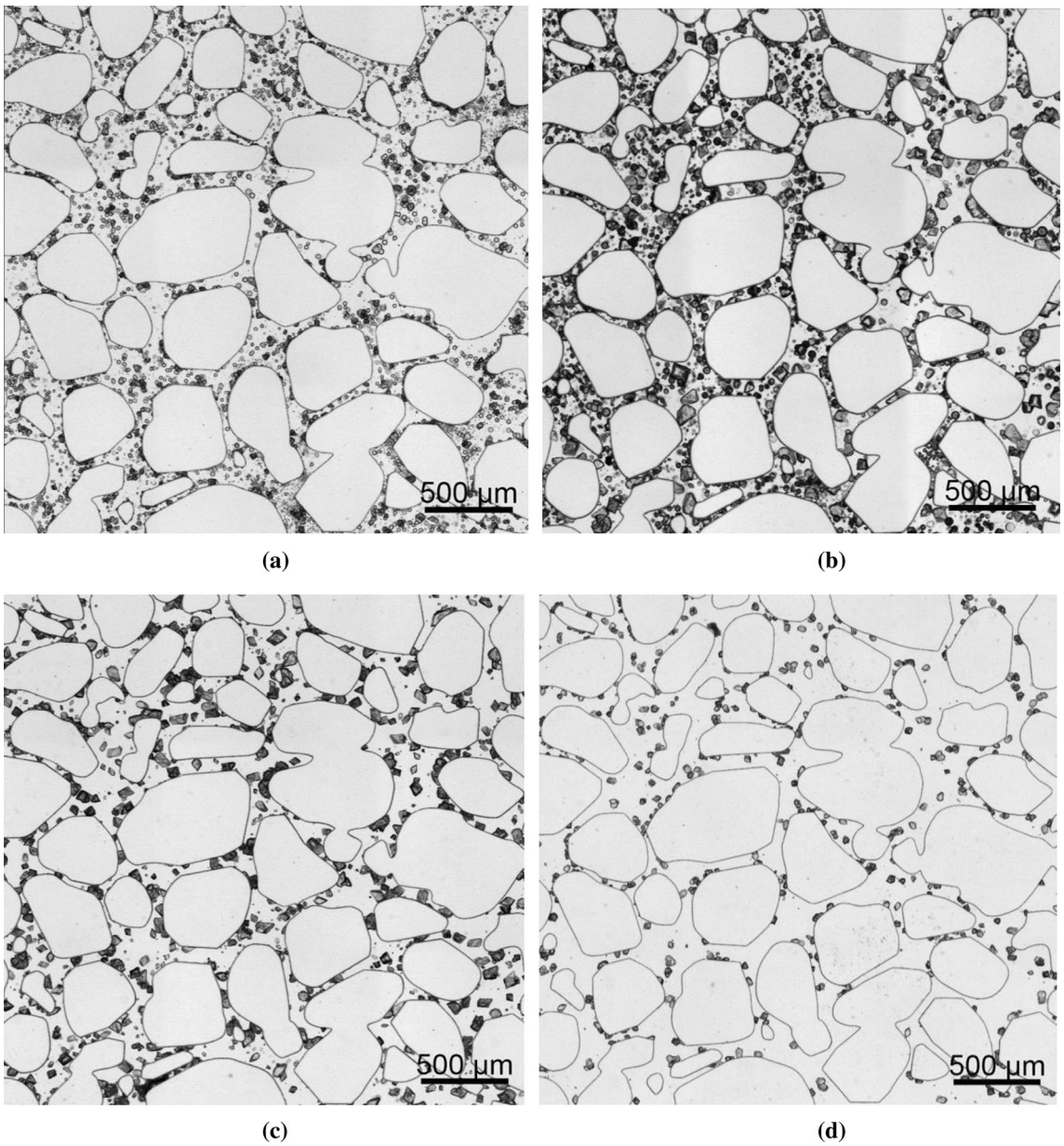

Fig. 11 3 mm by 3 mm microscope images taken at the central of the microfluidic chips taken at the completion of the MICP treatments. **a** 4 °C, **b** 20 °C, **c** 35 °C, **d** 50 °C

precipitation rate and chemical transform efficiency, but the crystals would be larger in amount and smaller in size. Therefore, compared to the high-temperature condition which is easier to optimize by introducing larger numbers of bacterial injections, the optimization of MICP treatment procedures at low temperatures is more challenging and will therefore require further investigations.

Previous studies conducted at room temperature normally considered the initial urease activity (which affects the precipitation rate) when determining the injection interval for MICP treatment protocols [2, 36, 38]. However, the findings presented in the current study illustrate that while urease activity may decrease quickly with time during the MICP treatment procedure, the initial urease activity cannot predict the precipitation rate of the whole process due to reasons such as temperature. In addition, the result at 50 °C also indicates that the main reason why the crystals stopped growing after the 4th injection was because the urease activity was zero, with extra bacterial supply being required to maintain the required urease activity in the precipitation system.

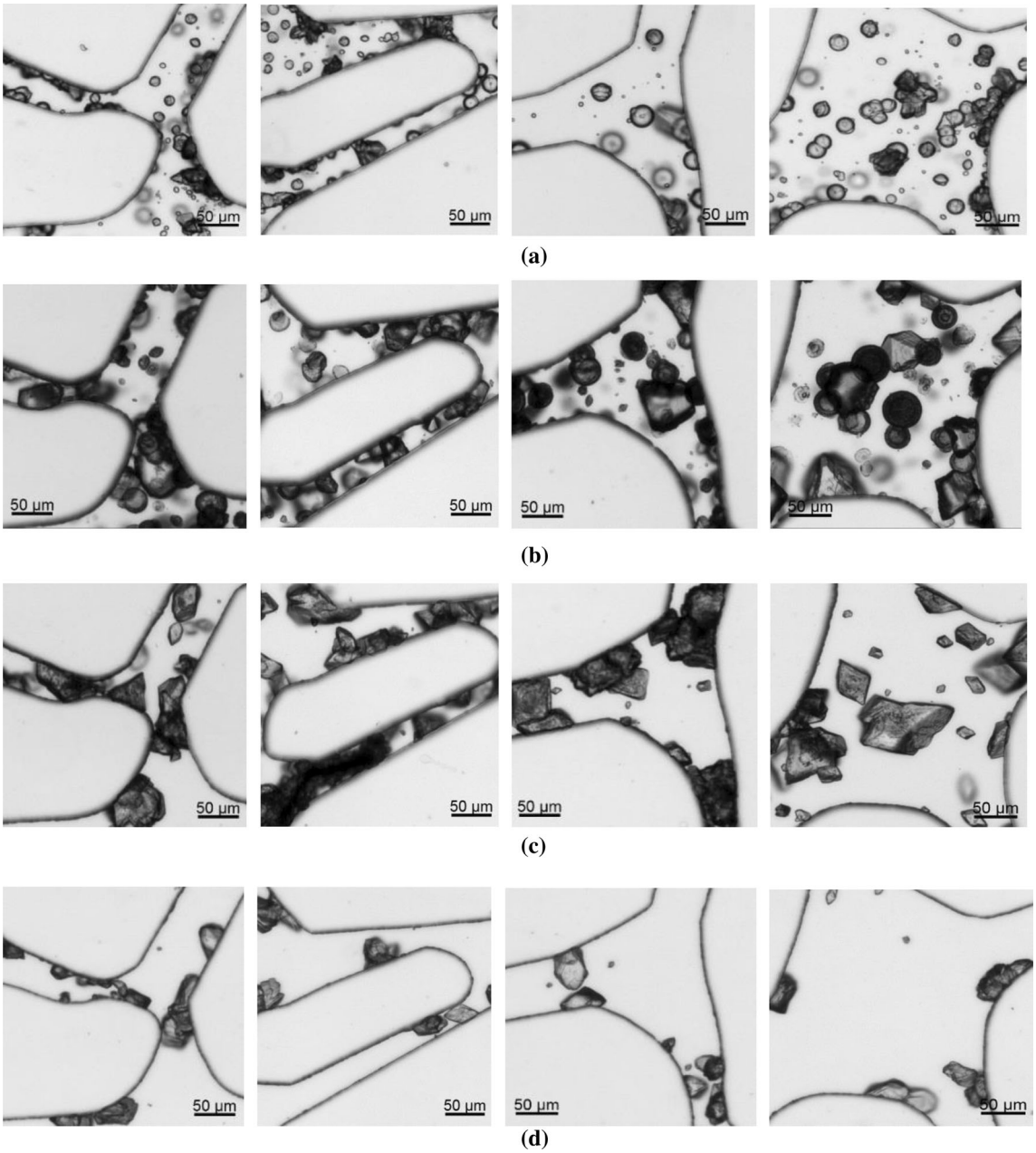

Fig. 12 magnified images at four pores in images shown in Fig. 11. **a** 4 °C, **b** 20 °C, **c** 35 °C **d** 50 °C

4 Conclusions

In this study, urease activity batch tests and microfluidic chip experiments were conducted to investigate the effects of temperature on urease activity, bacterial number, crystal growth, crystal dissolution, crystal characteristics and the chemical transform efficiency of MICP. The reasons for the low crystal growth rates at low and high temperatures are detailed and a method of optimizing MICP at high temperatures is proposed. These findings made from the microscope images have implications for better understanding of the MICP mechanisms at various temperatures and could be valuable for improving the MICP process for different applications. The main findings are as follows.

The effects of temperature on MICP crystal growth and efficiencies can be divided into the indirect and direct effects. The indirect ones refer to the effects of temperature on bacterial growth, attachment and ureolysis activity, which in turn influence the supersaturation condition of $CaCO_3$ precipitation. Direct one refers to the effect of temperature on $CaCO_3$ precipitation directly. The relatively low crystal precipitation rates and chemical efficiencies at 4 °C are mainly affected by the low bacterial number and low precipitation rate of $CaCO_3$ at low temperature. The

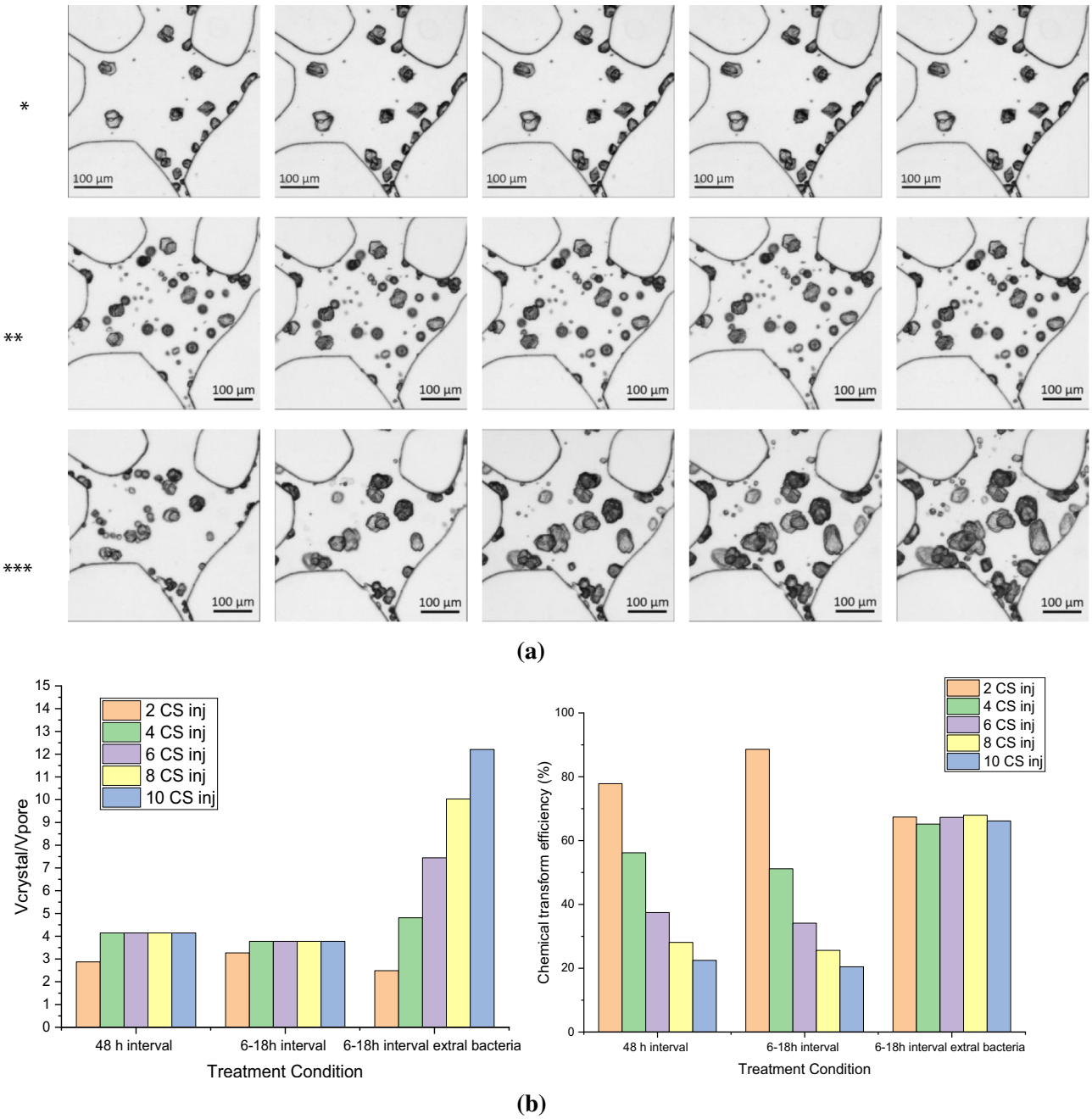

Fig. 13 Microscope images of one central pore of the microfluidic chips taken at the completion of the injection intervals of the second, fourth, eighth and tenth injections of cementation solution for the sample treated by an injection interval of 48 h (*), 6–18 h (*) and 6–18 h with bacterial injection before every two injections of cementation solution; **b** total crystal volume/pore volume vs injection number of cementation solution; **c** chemical transform efficiency vs injection number of cementation solution

relatively high crystal precipitation rates and chemical efficiencies at 20 °C are mainly due to the relatively higher number of bacterial cells after growth and detachment, and relatively higher overall crystals precipitation rate, which were not greatly affected by temperature. The higher initial crystal precipitation rate and chemical transform efficiencies at 35 °C is the same as for 20 °C. At 50 °C, the reductions of crystal precipitation rate and chemical transform in a larger range of precipitation time (2–10 injections) are mainly because of the quick reduction rates in urease activity at 50 °C.

The effects of temperature on $CaCO_3$ morphology are related to different crystal dissolution behavior of $CaCO_3$ at different temperatures. The dissolution of vaterite and reprecipitation into larger vaterite or calcite follows the Ostwald law of crystal growth and a rise in temperature

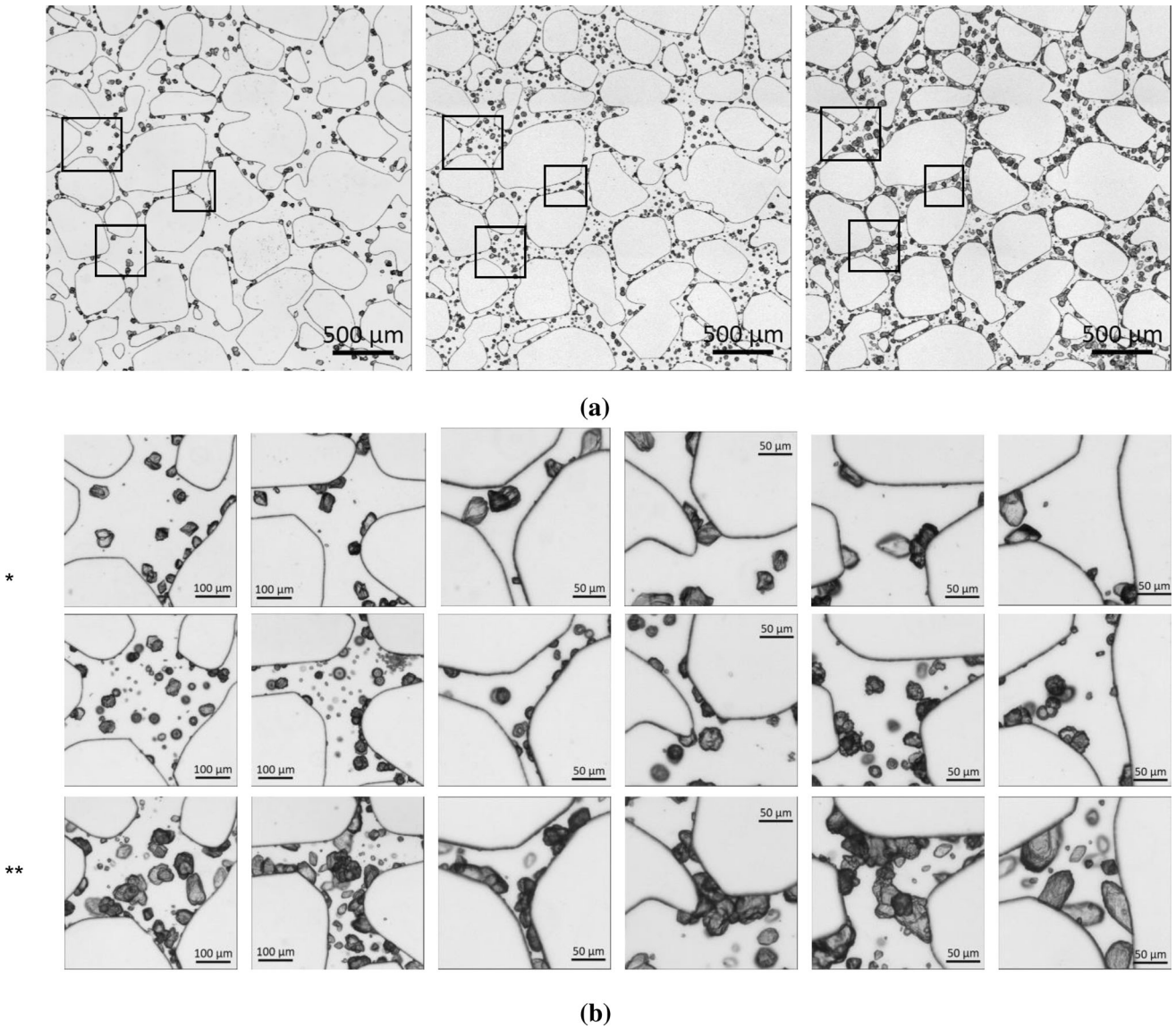

Fig. 14 **a** 3 mm by 3 mm microscope images taken at the central of the microfluidic chips taken at the completion of the MICP treatments at temperature of 50 °C and an injection interval of 48 h (left image), 6–18 h (middle image) and 6–18 h with extra injections of bacterial suspension before every other injections of cementation solution (right image); **b** magnified images at six pores in image (**a**)

increases the rate of transformation. Therefore, high-temperature conditions enhance the formation of calcite, whereas low-temperature conditions enhance the formation of vaterite. This study also observed a 'memory-like' effect for the crystal–dissolution–reprecipitation process. When a new batch of cementation solution is injected, the crystals tend to reprecipitate where the crystals used to be during the previous injection before they dissolved. This is probably because the crystal lattice remained on the channel surface of the porous medium, which provide less energy for nucleation to occur compared to nuclear on clean surface.

Although initial precipitation rate increases exponentially with temperature increase, the precipitation efficiency of MICP at 50 °C (Test 4) is very low because the high temperature reduces bacterial density and activity. At high temperature, therefore, increasing the injection number of bacterial suspension from 1 to 5 (Test 6) was found to be effective in increasing the $CaCO_3$ precipitation rate and chemical transform efficiency.

At low temperature, the low precipitation rate and chemical transformation efficiency are mainly because of the low $CaCO_3$ precipitation rate. The increasing bacterial density at low temperature may increase both precipitation rate and chemical transformation efficiency of MICP and the low temperature promotes the precipitation of a larger number of smaller crystals. However, the reduced $CaCO_3$ phase transformation rate would result in less effective

crystals in bonding soil particles. The optimization of MICP for soil strength enhancement at low temperature is more challenging and requires further investigations.

Acknowledgements Y.W. acknowledges the financial support of Natural Science Foundation of China (Grant Nos. 52171262, 42141003), Science and Technology Innovation Committee of Shenzhen (Grant No. JCYJ20210324103812033) and Shenzhen Key Laboratory of Natural Gas Hydrates (Grant No. ZDSYS20200421111201738) for conducting this study. The authors acknowledge Dr. Fedir Kiskin for proof reading the manuscript.

Author contributions The manuscript was written through contributions of all authors. All authors have given approval to the final version of the manuscript.

Data availability All data generated or analyzed during this study are included in this published article.

References

1. Achal V, Pan X, Zhang D (2011) Remediation of copper-contaminated soil by *Kocuria flava* CR1, based on microbially induced calcite precipitation. Ecol Eng 37:1601–1605. https://doi.org/10.1016/j.ecoleng.2011.06.008
2. Al Qabany A, Soga K (2013) Effect of chemical treatment used in MICP on engineering properties of cemented soils. Géotechnique 63(4):331–339. https://doi.org/10.1680/geot.SIP13.P.022
3. American Society for testing and materials, standard test methods for electrical conductivity and resistivity of water, D1125–D1195
4. Bachmeier KL, Williams AE, Warmington JR, Bang SS (2002) Urease activity in microbiologically-induced calcite precipitation. J Biotechnol 93(2):171–181. https://doi.org/10.1016/S0168-1656(01)00393-5
5. Barron JJ, Ashton C (2005) The effect of temperature on conductivity measurement, TSP, knowledge.reagecon.com
6. Changnon SA (1999) A rare long record of deep soil temperatures defines temporal temperature changes and an urban heat island. Clim Change 42(3):531–538. https://doi.org/10.1023/a:1005453217967
7. Cheng L, Cord-Ruwisch R (2014) Upscaling effects of soil improvement by microbially induced calcite precipitation by surface percolation. Geomicrobiol J 31(5):396–406
8. Cheng L, Shahin MA, Mujah D (2017) Influence of key environmental conditions on microbially induced cementation for soil stabilization. J Geotech Geoenviron Eng 143(1):04016083. https://doi.org/10.1061/(asce)gt.1943-5606.0001586
9. Chow TT, Long H, Mok HY, Li KW (2011) Estimation of soil temperature profile in Hong Kong from climatic variables. Energy Build 43(12):3568–3575. https://doi.org/10.1016/j.enbuild.2011.09.026
10. Chu DH, Vinoba M, Bhagiyalakshmi M, Hyun Baek I, Nam SC, Yoon Y, Jeong SK (2013) CO232 system. RSC Adv 3(44):21722. https://doi.org/10.1039/c3ra44007a
11. Cöelfen H, Antonietti M (2008) Mesocrystals and nonclassical crystallization. Wiley, Hoboken
12. DeJong JT, Mortensen BM, Martinez BC, Nelson DC (2010) Bio-mediated soil improvement. Ecol Eng 36(2):197–210
13. Dinghua P, Suyu Q, Yao L, Hang Ma, Lei Z, Hou Siyu Wu, Heng BX (2020) Performance of microbial induced carbonate precipitation for immobilizing Cd in water and soil. J Hazard Mater 400:123116
14. Dunne WM (2002) Bacterial adhesion: seen any good biofilms lately? Clin Microbiol Rev 15(2):155–166
15. Dupraz S, Parmentier M, Ménez B, Guyot F (2009) Experimental and numerical modeling of bacterially induced pH increase and calcite precipitation in saline aquifers. Chem Geol 265(1–2):44–53
16. Fathima F, Jayalakshmi S (2012) Characterization of urease enzyme from marine bacterium Klebsiella species. Afr J Microbiol Res 6:5914–5923
17. Ferris FG, Phoenix V, Fujita Y (2004) Kinetics of calcite precipitation induced by ureolytic bacteria at 10 to 20 °C in artificial groundwater. Geochim Cosmochim Acta 68(8):1701–1710
18. Gao Z, Bian L, Hu Y, Wang L, Fan J (2007) Determination of soil temperature in an arid region. J Arid Environ 71(2):157–168
19. Green FHW, Harding RJ (1980) Altitudinal gradients of soil temperatures in Europe. Trans Inst Br Geogr 5(2):243–254
20. Han P, Geng W, Li M, Jia S, Yin J, Xue R (2021) Improvement of biomineralization of sporosarcina pasteurii as biocementing material for concrete repair by atmospheric and room temperature plasma mutagenesis and response surface methodology. J Microbiol Biotechnol 31(9):1311–1322
21. Hataf N, Baharifard A (2020) Reducing soil permeability using microbial induced carbonate precipitation (MICP) method: a case study of shiraz landfill soil. Geomicrobiol J 37(2):147–158. https://doi.org/10.1080/01490451.2019.1678703
22. Khan YM, Munir H, Anwar Z (2019) Optimization of process variables for enhanced production of urease by indigenous Aspergillus niger strains through response surface methodology. Biocatal Agric Biotechnol 20(April):101202
23. Koh CA, Westacott RE, Zhang W, Hirachand K, Creek JL, Soper AK (2002) Mechanisms of gas hydrate formation and inhibition. Fluid Phase Equilib 194:143–151
24. Kralj D, Brečević L, Kontrec J (1997) Vaterite growth and dissolution in aqueous solution III. Kinetics of transformation. J Crys Growth 177(3–4):248–257
25. Mitchell AC, Phillips AJ, Hiebert R (2009) Biofilm enhanced geologic sequestration of supercritical CO_2. Int J Greenhouse Gas Control 3(1):90–99
26. Mortensen BM, Haber MJ, DeJong JT (2011) Effects of environmental factors on microbial induced calcium carbonate precipitation. J Appl Microbiol 111(2):338–349
27. Nemati M, Voordouw G (2003) Modification of porous media permeability, using calcium carbonate produced enzymatically in situ. Enzyme Microb Technol 33:635–642
28. Ning-Jun J, Liu Rui Du, Yan-Jun B-Z (2019) Microbial induced carbonate precipitation for immobilizing Pb contaminants: toxic effects on urease activity and immobilization efficiency. Sci Total Environ 672:722–731. https://doi.org/10.1016/j.scitotenv.2019.03.294
29. van Paassen LA, Ghose R, van der Linden Thomas JM, van der Star Wouter RL, van Loosdrecht Mark CM (2010) Quantifying biomediated ground improvement by ureolysis: large-scale biogrout experiment. J Geotech Geoenviron Eng 136(2):1721–1728
30. Peltzer ET, Brewer PG (2000) Practical physical chemistry and empirical predictions of methane hydrate stability. Natural Gas Hydrate. Springer, Dordrecht, pp 17–28
31. Peng J, Liu Z (2019) Influence of temperature on microbially induced calcium carbonate precipitation for soil treatment. PLoS ONE 14(6):e0218396
32. Sagidullin AK, Stoporev AS, Manakov AY (2019) Effect of temperature on the rate of methane hydrate nucleation in water-in-crude oil emulsion. Energy Fuels 33(4):3155–3161
33. Stocks-Fischer S, Galinat JK, Bang S (1999) Microbiological precipitation of $CaCO_3$. Soil Biological Biochemistry 31(11):1563–1571

34. Sun X, Miao L, Tong T, Wang C (2018) Study of the effect of temperature on microbially induced carbonate precipitation. Acta Geotech 14(3):627–638
35. Wang Y, Konstantinou C, Soga K, Biscontin G, Kabla AJ (2022) Use of microfluidic experiments to optimize MICP treatment protocols for effective strength enhancement of MICP-treated sandy soils. Acta Geotech. https://doi.org/10.1007/s11440-022-01478-9
36. Wang Y, Soga K, DeJong JT, Kabla AJ (2019) Microscale visualization of microbial-induced calcium carbonate precipitation processes. J Geotech Geoenviron Eng 145(9):04019045
37. Wang Y, Soga K, DeJong JT, Kabla AJ (2021) Effects of bacterial density on growth rate and characteristics of microbial-induced $CaCO_3$ precipitates: particle-scale experimental study. J Geotech Geoenviron Eng 147(6):04021036
38. Wang Y, Soga K, Dejong JT, Kabla AJ (2019) A microfluidic chip and its use in characterising the particle-scale behaviour of microbial-induced calcium carbonate precipitation (MICP). Géotechnique 69(12):1086–1094
39. Wang Y, Soga K, Jiang NJ (2017) Microbial induced carbonate precipitation (MICP): the case for microscale perspective. In Proceedings of the 19th international conference on soil mechanics and geotechnical engineering, pp. 1099–1102
40. Whiffin VS, van Paassen LA, Harkes MP (2007) Microbial carbonate precipitation as a soil improvement technique. Geomicrobiol J 24(5):417–423
41. Whiffin VS (2004) Microbial $CaCO_3$ precipitation for the production of biocement (Doctoral dissertation, Murdoch University)
42. Wu L, Zhang J (2014) Strong subsurface soil temperature feedbacks on summer climate variability over the arid/semi-arid regions of East Asia. Atmosp Sci Lett 15(4):307–313
43. Xiao Y, He X, Wu W, Stuedlein AW, Evans TM, Chu J, Hanlong LH, van Paassen LA, Wu H (2021) Kinetic biomineralization through microfluidic chip tests. Acta Geotech 16:3229–3237
44. Xiao Y, He X, Stuedlein AW, Chu JT, Evans TM, van Paassen LA (2022) Crystal Growth of MICP through Microfluidic Chip Tests. J. Geotech. Geoenviron. Eng., 2022, 148(5): 06022002
45. Zhang W, Ju Y, Zong Y, Qi H, Zhao K (2018) In situ real-time study on dynamics of microbially induced calcium carbonate precipitation at a single-cell level. Environ Sci Technol 52(16):9266–9276
46. Zhao Q (2014) Experimental study on soil improvement using Microbial Induced Calcite Precipitation (MICP). Beijing: China University of Geoscience (Beijing)